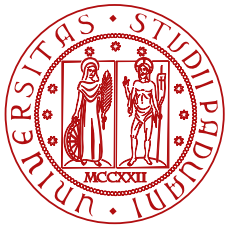

Università degli Studi di Padova

Dipartimento di Ingegneria Industriale

Master Thesis in Electrical Energy Engeneering

The role of the electric transmission grid in the decarbonization process of the Italian power sector

Master Candidate

Stefano Grazian

Student ID 2016759

Supervisor

Prof. Giuseppe Zollino

University of Padova

Co-supervisor

Eng. Chiara Bustreo

Consorzio RFX

Academic Year
2021/2022

"Multa, non quia difficilia sunt, non audemus, sed quia non audemus, sunt difficilia."
L. A. Seneca

Abstract

In recent years, the EU has adopted important and bold policies to tackle the problem of global warming and climate change: with the *Europen Green Deal*, all member states have pledged to reduce greenhouse gas emissions by 55% by 2030 compared to 1990 levels, and the ultimate goal is to make Europe the world's first climate-neutral continent by 2050. To achieve these challenging goals, decarbonization strategies have been developed that will lead to a radical change in the energy sector and in particular in the power sector: power generation will have to rely on intermittent and non-programmable renewable sources that will have to be supported by storage plants and strong reinforcement of the power grid. In this context, In this context, assessing the techno-economic viability of alternative energy scenarios play a crucial role. This thesis presents the COMESE, a code developed at the Consorzio RFX for modelling the operation of future power system, estimate costs and assessing the technical feasibility. In particular, the research work is focused on the effects of the Italian power sector evolution on the transmission grid requirements. Improvements have been introduced regarding both the technical and economic description of the power grid. Furthermore, the interaction between it and storage systems has been studied, implementing new alternatives for the model of sotrage operation in order to achieve more effective management of the generation fleet and improve code performance. The changes were applied to the study of Italian energy scenarios on the basis of the latest decarbonization policies and plans for the development of the power sector. Moreover the simulations were supported by the use of an optimization algorithm in order to find the optimal (least-cost) configuration of the electricity system, while ensuring the achievement of decarbonization targets and the balancing of the demand. Finally, the possible integration of nuclear fusion into the electricity mix was studied, investigating the technical and economic impacts such plants could have in a system with a very high share of photovoltaic and wind power.

Sommario

Negli ultimi anni l'UE ha adottato politiche importanti e coraggiose per affrontare il problema del riscaldamento globale e del cambiamento climatico: con il Green Deal europeo tutti gli Stati membri si sono impegnati a ridurre le emissioni di gas serra del 55% entro il 2030 rispetto ai livelli del 1990, e l'obiettivo finale è rendere l'Europa il primo continente climaticamente neutro entro il 2050. Per raggiungere questi sfidanti obbiettivi sono state sviluppate strategie di decarbonizzazione che porteranno ad una radicale modifica del settore energetico ed in particolare del sistema elettrico: la generazione dovrà essere affidata a fonti rinnovabili intermittenti e non programmabili che dovranno essere affiancate da impianti di accumulo ed un forte rafforzamento della rete elettrica. In questo contesto è importante disporre di strumenti in grado di valutare la fattibilità tecno-economica dei diversi scenari energetici: in questa tesi si presenta il codice CO.ME.S.E., sviluppato al *Consorzio RFX* e utilizzato per indagare il funzionamento dei futuri sistemi elettrici e il relativo costo medio dell'energia. In particolare, il lavoro di ricerca si è concentrato sugli effetti che l'evoluzione del settore elettrico italiano comporta sui requisiti della rete di trasmissione. Sono stati introdotti miglioramenti riguardanti sia la descrizione tecnica che economica della rete elettrica, inoltre è stata studiata l'interazione tra essa e i sistemi di accumulo, implementando nuove alternative per il modello di quest'ultimi impianti in modo da ottenere una gestione più efficace del parco di generazione e migliorare le performance del codice. Le modifiche apportate sono state applicate allo studio di scenari energetici italiani riguardanti le più recenti politiche di decarbonizzazione e piani di sviluppo del sistema elettrico. Inoltre le simulazioni sono state affiancate dall'utilizzo di un algoritmo di ottimizzazione in modo da trovare la configurazione ottimale (a minor costo) del sistema elettrico, garantendo allo stesso tempo il raggiungimento dei target di decarbonizzazione e il soddisfacimento della domanda. Infine è stata studiata la possibile integrazione della fusione nucleare nel mix elettrico, indagando l'impatto tecno-economico che tali impianti potranno avere in un sistema che presenta un'elevata quota di fotovoltaico ed eolico.

Contents

List of Figures

List of Tables

Nomenclature

Indices and Acronym

BioGas BioGas-fired power plants.

BMR Baseload and Must Run.

CCUS Carbon Capture Utilization and Storage.

Co Costs.

DE Differential Evolution.

EHd Equivalent Hours distribution.

Geo Geothermal.

HVAC High Voltage Alternating Current.

HVDC High Voltage Direct Current.

HyDam water-reservoir hydropower power plants.

LCOTE Levelized Cost of Timely Electricity.

MSW Municipal Solid Waste.

O&M Operation and Maintenance.

OffSW Off-Shore floating Wind.

OG Over-Generation.

OHL Over-the-Head Line.

OnSW On-Shore floating Wind.

PdS Piano di Sviluppo.

PHS Pumped Hydro Storage.

PV Photovoltaic.

RES Renewable Energy Sources.

RGCd Request for Grid Connection distribution.

ROR Run-Of-the-River.

TSO Transmission System Operator.

h hours.

I Transmission grid Interconnection.

z zone.

Symbols

$\boldsymbol{A_{eq}}$ Equality constraints matrix.

$\boldsymbol{A}$ Inequality constraints matrix.

$\boldsymbol{b_{eq}}$ Equality constraints, right-hand-side.

$\boldsymbol{b}$ Inequality constraints, right-hand-side.

$\boldsymbol{C_M}$ Nodal matrix.

$\boldsymbol{l_b}$ Lower bounds.

$\boldsymbol{M_T}$ Incidence matrix.

$\boldsymbol{u_b}$ Upper bounds.

Cap Storage energy Capacity.

D Electric Demand.

Def Residual demand (Deficit).

E Energy.

G Fixed Generation profile.

h_c Storage charging hours.

h_e Full-load equivalent hours.

h_{FW} Hours of Forecast Interval.

h_{LTFW} Hours of Long Term Forecast Interval.

K Weight coefficient.

le Length of transmission line.

N_h Length of analysis horizon.

N_l Number of transmission lines.

N_{ss} Number of substations.

P Generated Power.

P_n Nominal Power.

Pch Charging Power, storage plants.

$Pdch$ Discharging Power, storage plants.

PF Power Flow.

$Surp$ Excess power or Surplus.

T_C Transmission capacity.

Chapter 1

Introduction

In the last century, together with the development of industrialized societies, there has been an exponential growth in the World's energy needs (see 1.1), which have mainly been satisfied by using non-renewable fossil fuels (gas, oil, and coal) responsible for the emission of large quantities of greenhouse gases into the atmosphere. In fact, if the same time interval is considered, the production of carbon dioxide due to human activities has grown significantly and there is now a widespread consensus among the scientific community in affirming that this has serious influences on climate: the concentration of CO2 in the atmosphere has undergone a steep increase leading to a rise in the global average temperature. On the other hand, in recent years, more and more interest and attention have been paid to this issue also by the stakeholder: numerous states have reiterated the seriousness of the problem and the need to implement urgent measures to tackle climate change. In this context, the European Union (EU), following up on commitments made in the 2015 Paris Agreements, has taken on a global leadership role: in December 2019 the European Commission issued the European Green Deal with which it aims to *"transform the EU into a fair and prosperous society, with a modern, resource-efficient and competitive economy where there are no net emissions of greenhouse gases in 2050 and where economic growth is decoupled from resource use"* [2]. Furthermore, the dramatic war in Ukraine has once again highlighted, among other things, the need to have an energy mix that is as independent as possible from the import of fossil fuels and flexible to external geopolitical upheavals. The goal of achieving carbon neutrality by 2050, with an intermediate step to 2030 which foresees a 55% reduction in greenhouse gas emissions compared to 1990 levels, appears very bold and challenging, considering the relatively short time available: the entire energy sector should undergo a radical transformation facing technical and economical issues

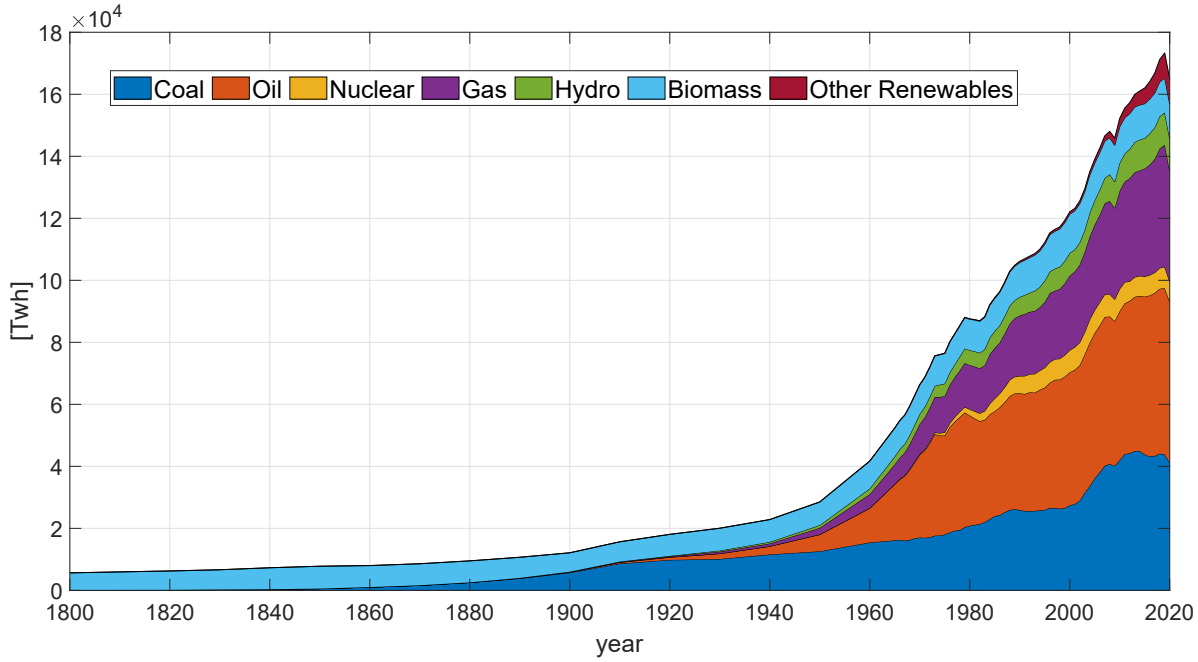

Figure 1.1: Primary energy consumption by fuel. Data taken from [28] and [12]

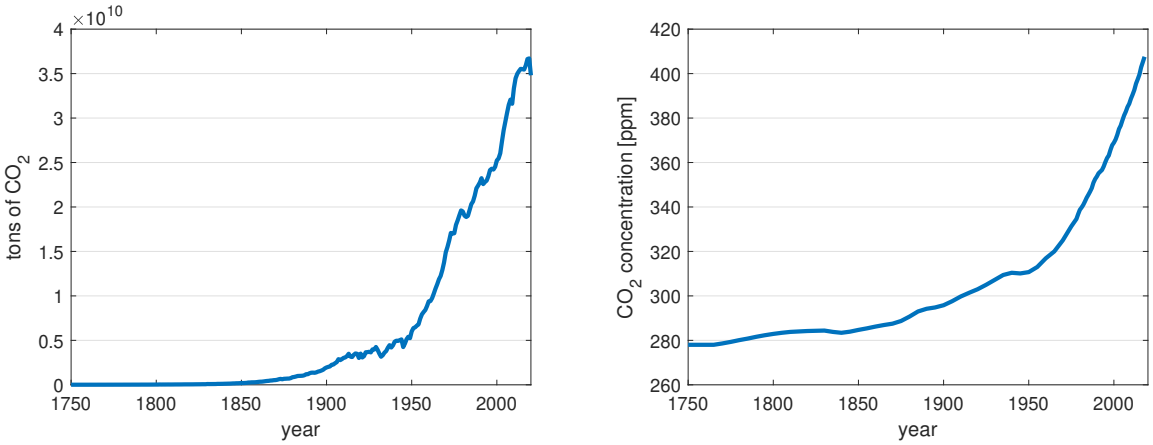

Figure 1.2: Carbon dioxide emission due to human activities (left figure) and carbon dioxide concentration in the atmosphere (right figure). Source: Our World in Data [8]

never experienced before.

1.1 The decarbonisation of the Italian power sector

Italy has also committed itself to follow the European Commission's directives by defining energy targets and the measures to achieve them in two important documents: the PNIEC (Piano Nazionale Integrato per l'Energia e il Clima, i.e.Integrated National Energy and Climate Plan) [24] and the "Strategia Italiana di lungo termine sulla riduzione delle emissioni di gas serra" [30] ("Italian long-term strategy for the reduction of greenhouse gas emissions"). In the former, targets are set for 2030, which can be summarised as follows: a 30% share of energy from renewable energy sources (RES) in Gross Final Energy Consumption, of which 55% in the electricity sector, 34% in heating and 22% in transports. Specifically, these objectives translate into the complete phase-out from coal by 2025, and the coverage by 2030 of more than half of gross electricity consumption (55%) by RES as shown in figure 1.3). This will require the in-

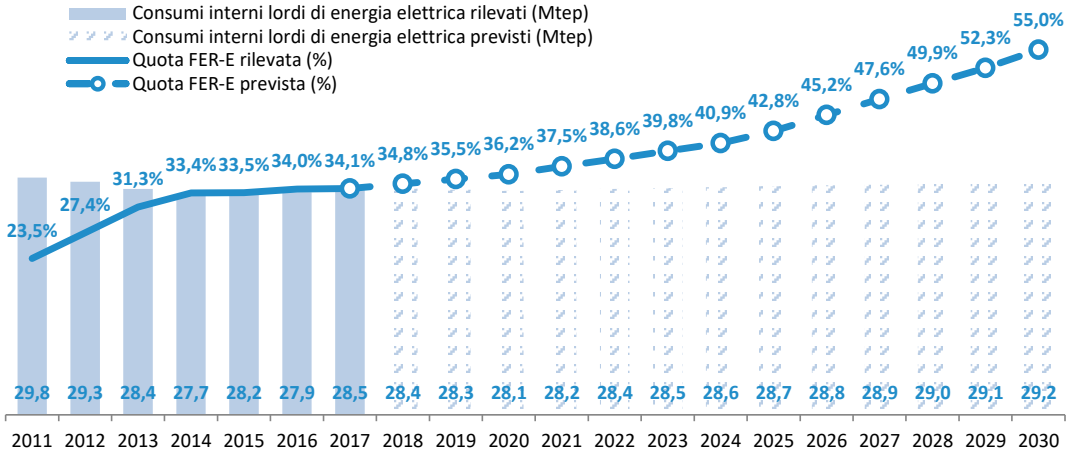

Figure 1.3: RES share in the Italian electricity mix. Source: GSE, RSE

stallation by 2030 of about 40 GW of new RES capacity, supplied almost exclusively by non-programmable renewable sources such as wind and photovoltaics. What's more, the new road-map defined by the EU Commission with the Green Deal implies that the already challenging targets for the penetration of renewables in electricity consumption defined in the PNIEC will have to be reformulated in an even more ambitious way: Italy will likely have to reach a 65% RES share in the electricity sector, which would require the installation of at least further 20 GW of photovoltaic and wind power compared to what was already been identified by the PNIEC. The "Italian long-term strategy for the reduction of greenhouse gas emissions" identifies the possible pathways to reach

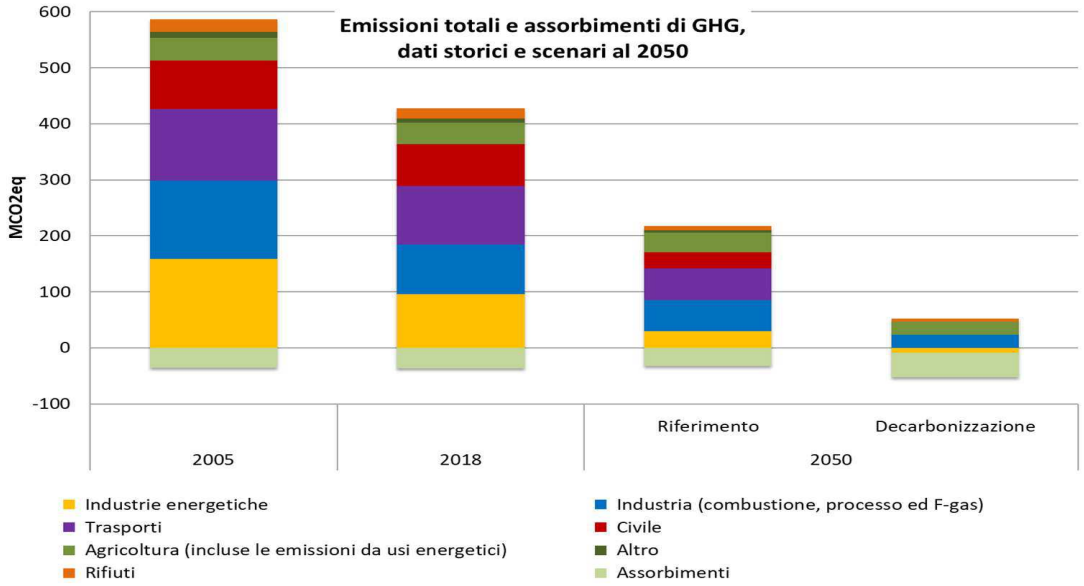

Figure 1.4: Total emissions and absorption of GHG, historical data and 2050 scenarios. Source: ISPRA

a 'climate neutrality' condition by 2050 (figure 1.4), guaranteeing, at the same time, an adequate level of security and affordability in the energy supply. In particular, it is highlighted that it will be necessary to increase the efficiency in the final energy conversion in order to reduce the energy demand, to change radically the energy mix in favor of renewable sources together with deep electrification of consumption, and to use forms of CCUS (Carbon Capture Utilization and Storage). Furthermore, not only will electricity have to be produced (almost) exclusively from renewable sources, but it will be necessary to install storage systems for a total power of 30-40 GW and to develop efficient technologies to produce fuels (such as hydrogen) using the excess energy coming from non-programmable plants.

So, the main player in this transition will certainly be the power sector because, within current energy policies, it is the one where the largest reductions in greenhouse gas emissions are planned to be achieved and it will be essential to reach the decarbonisation targets in other sectors as well. This is due to the fact that the production of electricity, which is currently responsible for about 40% of total carbon dioxide emissions, is well suited to the integration of renewable energy plants, which are becoming more and more economically competitive and whose share is destined to increase significantly in the coming years. Moreover, the conversion of electricity into other energy services generally takes place with much higher efficiencies than the corresponding fuel-based applications, therefore, to reduce greenhouse gas emissions, greater electri-

fication of final consumption will be required. In particular this will affect the heating and transport sectors, thanks to the spread of efficient technologies such as heat pumps and electric vehicles. On the other hand, the decarbonization process implies for the power sector a deep transformation with never-before-experienced technical and operational complexities. First of all, it will be more complex to ensure the instantaneous balance between electric generation and demand, due to the high intermittency of RES. The total nominal capacity of RES plants is expected to be significantly higher than the demand peak, leading to periods of overgeneration, and, at the same time, storage systems along with other dispatchable technologies will have to be introduced to cope with situations of low generation and steep drops in power coming from RES. Then, there will be a progressive reduction of the frequency response capability and grid inertia, due to the increase of non-programmable generators connected to the grid by means of static converters. Furthermore, RES will also be unevenly distributed across the country, depending on the availability of resources, and it is not unlikely that the major areas of consumption will be relatively far from where electricity is mainly produced. These facts will lead to an increase in grid congestion events and a worsening of voltage and frequency regulation issues [23]. So, major investments will also be needed to strengthen and improve the electricity grid. For example, Terna, the Italian TSO, in its Piano di Sviluppo 2021 (2021 Development Plant) [23] has defined a plan of 18 billion over 10 years.

1.2 Energy models and scenarios

Research on energy scenarios proves to be central in this context in order to guide the investment decisions of regulators and system operators. First of all, a distinction must be made between forecasts and scenarios: the former are predictions about an event or condition using quantitative historical methods, i.e. they rely mainly on data from the present or the past. Scenarios, unlike forecasts, consist of a set of coherent assumptions about the future trajectories of energy-relevant drivers, leading to a coherent organization of the system under study. In other words, energy scenarios are not predictions of the future characteristics of the energy system, but rather indicators of what outcomes or effects the application of certain policies and the occurrence of assumptions (set as input data) may have.

Several tools that perform scenario analysis already exist (a large number of example can be found in [3] and [6], but often they can't provide a complete picture of the system

under analysis because of the intrinsic complexity of the problem, and the great number of variables involved in a study of this kind [17]: various codes, both open-source and commercial, have been developed for the study of scenarios, but each one with its own characteristics and designed to emphasise a particular facet of interest. Moreover, these tools can be based on significantly different approaches and it is not still well established which is the best way (if there is one) to face this type of analysis. Thus, is important to present at least a streamlined classification, dividing scenario models into two macro-categories.

Top-down models *"Top-down energy models try to depict the economy as a whole on a national or regional level and to assess the aggregated effects of energy and/or climate change policies in monetary units"* [3]. These models are based on general equilibrium equations (they seek to balance markets by maximising consumer welfare) and take an aggregate view of energy sectors and the economy, thus they can simulate future energy demand and supply, together with the impacts on economic growth, employment or foreign trade. However, they rely heavily on price trends and financial policies, but lack a detailed techno-economic description of the system under analysis, so they are not suitable for describing the development of specific technologies or sectoral policies at an exhaustive level.

Bottom-up models Bottom-up models are so called because they usually focus only on the energy sector of an economy, using a high degree of techno-economic detail to study the system under analysis: each subdivision consists of a relatively large number of technologies that are logically organised and linked together through precise relationships, and each technology is identified by a detailed description of its inputs, outputs, unit costs, and other characteristics. Consequently, these models are suitable for assessing the impact of various technologies or specific policies in the energy sector, showing what the main issues or best alternatives might be, both in technical terms (relating to system operation) and economic terms (relating to costs) to achieve pre-determined goals. On the other hand, they do not take into account the mutual interaction between the energy sector and the remaining economic areas, and thus do not allow for an assessment of the macroeconomic effects of energy or climate policies and related investments.

In addition, other characteristics differentiate the various energy scenario models. For instance, following the classification made in [22]

- Spatial and time scale: The simulation may cover several years or focus on a more limited time window; if a large time interval is taken into account, the entire evolution of the energy system can be analysed, but usually a rather coarse temporal resolution is used, limited to few typical days during the year or to predefined 'time slices' considered relevant. Instead, hourly or even finer simulations allow very detailed analysis and are particularly suitable in systems with a large share of intermittent and non-programmable RES and storage technologies. On the other hand, to avoid an excessive computational burden, they are usually limited to the analysis of one year or shorter periods. Similarly, models can range from regional to global scales, but the wider the area of analysis, the less detailed the spatial analysis usually is. Of course, both approaches have their pros and cons, as analysing large areas of space allows one to study the interactions between them and obtain a broad and general picture, while focusing on a single nation or region leads to a more accurate simulation, given the evolution of energy systems from a centralised to a distributed structure.

- Considered energy sectors: As mentioned above, increasing interaction between the various energy sectors (power sector, transport, heating...) is to be expected in the near future, so various models have been developed to consider the entire energy system and sector-coupling. Often, however, the degree of detail of the individual sectors is not high enough, or at any rate not close to that of models that focus on a single sector. The power sector, in particular, is the one mainly affected by decarbonisation policies and will undergo to a radical transformation, acting as a guide and support for the other energy sectors as well: the high share of renewables, the presence of storage systems, and the interaction with the grid necessitate the use of an adequate model.

- Simulation vs optimization: Finally, an important distinction should be made between models that perform only the simulation of a system with fixed inputs, and the ones that carry out an optimization having one or several parameters to be optimized in order to find the best configuration (in terms of costs, emission) for a given energy system.

In this thesis the COMESE code will be presented and extensively used to study long term decarbonisation scenarios of the Italian power sector: this tool performs a detailed hourly simulation of the whole power system and compute the related average system costs, so as to have a complete techno-economic assessment of the scenario under

analysis. Moreover it can also be matched with a differential evolution optimization algorithm, which provides useful information regarding the optimal configuration of the energy mix needed to reach the ambitious target of carbon neutrality.

Chapter 2

COMESE code

CO.ME.S.E. (COsto MEdio del Sistema Elettrico, Average Cost of the Electric System) is a MATLAB code created as part of the research activities on energy scenarios at RFX Consortium in Padua. It was developed to evaluate the techno-economic implications of decarbonization strategies concerning the power sector. In particular, the operation of the generation fleet of a geographic area, usually a country, is analyzed by performing a simulation on an hourly basis over an entire solar year; this temporal resolution, as well as the analysis time span. Although they can be varied by the user, reflect the characteristics of the data made available by the various TSOs (transmission system operators). Moreover, as mentioned earlier, the latest energy scenarios involve a very high share of generation from renewable, non-programmable, and intermittent sources, along with the installation of significant storage system capacity: in order to effectively assess the impact of these technologies, it is necessary to analyze a sufficiently long time interval with high temporal resolution.

Depending on the user's needs, the representation of the electrical system may have different degrees of detail: in the "copper-plate" mode, which is equivalent to assuming that the electric grid has infinite capacity and is losses-free, generation and storage facilities are aggregated by types and combined into a single node, to which the load representing the entire final electric demand is also connected. On the other hand, the power system can be split into several zones (nodes) linked by transmission lines with finite capacity; in this way, critical grid connections are identified, while the single zones are modelled as "copper-plate". A significant example is the zonal representation used by the electric market operator, where Italy is split into 6 zones: North (N), Centre-North (CN), Centre-South (CS), South (S), Sicily (Sic), Sardinia (Sar) [16]. Obviously the "copper-plate" approach can be seen as a particular case of the zonal approach,

consequently we will concentrate on the description of the code in its most general form.

The logic of managing the various plants is not based on simulating the dynamics of the electricity market; in fact, the main objective of the code is to meet the demand by following a fixed unit commitment of the various technologies, aimed at obtaining a system with the lowest average cost and efficient dispatching. At the end of the simulation, LCOTE (Levelized Cost Of Timely Electricity) is computed, which is the parameter used to evaluate the "system" cost and compare the various scenarios or different configurations of the electricity mix from an economic point of view. It is worth saying that the LCOTE is an economic indicator to be used for scenarios comparison rather than for the estimation of the future cost of electricity.

A unique feature of COMESE is the user's ability to define the length of a "forecast interval": thus the code, for each hour of the year, determines the optimal dispatch by looking at what the system behavior will be in a given number of future hours. Typically an entire day (24 hours) is chosen as the forecast interval, because it has been verified that further increasing this parameter does not lead to significant changes on the final results. Moreover it resembles the structure of the Italian electricity market.

To sum up, the characteristics presented make COMESE a valid simulation software, which determines the hourly operation of a system with fixed inputs, while the cost of electricity is calculated ex-post, without influencing the characteristics of the system studied, nor the criteria of management of various technologies. However, there is also the possibility of coupling the code to an optimization algorithm that automatically varies the values of a set of input variables (within a defined range) in order to find the configuration of the electrical mix that minimizes the LCOTE.

In this chapter the various sections of the code will be described in detail, while in the following one, modifications and improvements implemented during the thesis work will be presented.

2.1 COMESE Input

The data needed to run the simulation can be grouped as follows.

- Time parameters (defined by a number of hours):
  - length of analysis horizon N_h (usually 8760 hours)
  - length of forecast interval h_{FW} (usually 24 hours)
  - length of Long Term forecast interval $h_{LT\,FW}$ (usually 365 hours); it's used to define a rough allocation of the available energy of dispatchable plants, as explained in section 2.2.1.

- Characterization of generation and storage plants. The various technologies are divided into 5 macro-typologies:

  1→ technologies with fixed generation profile. The nominal power (Pn) and equivalent full-load hours must be defined for each zone. Alternatively, the annual energy yield and the full-load equivalent hours (h_e) must be specified, in fact

  $$Pn = E_y/h_e \tag{2.1.1}$$

  2→ technologies with a constant generation profile. The nominal power and equivalent full-load hours must be defined for each zone. Alternatively, the annual energy yield (E_y) and the full-load equivalent hours must be specified.

  3→ Energy-constrained dispatchable plants. The nominal power and maximum energy available in a year ($E_{disp\,tot}$) must be defined for each zone.

  4→ Energy-unconstrained dispatchable plants. The nominal power must be defined for each zone. It is also possible to define the maximum energy that can be produced in a year (usually a much higher value than that defined for plants of "type 3"); in this case it is sufficient to specify it for a single zone.

  5→ Storage plants. The nominal power and the charging time (h_c) must be defined for each zone and for each storage technology. Instead of the nominal power, one can specify the maximum storage capacity Cap:

  $$Pn_{stor} = Cap/h_c \tag{2.1.2}$$

- For each zone, the yearly energy Demand ($D_{z\,tot}$) and, eventually, the overall Import/Export energy.

- For each zone the Demand and Import/Export reference annual profile, and the reference annual generation profile of all the technologies belonging to "type 1".

- Economic data related to the different production and storage technologies
- Transmission grid characterization:
  - gird topology, defined by the square symmetric matrix $\boldsymbol{C_M}$. $\boldsymbol{C_M}$ has dimension $N_Z \times N_Z$ (where N_Z is the number of zones) and $\boldsymbol{C_M}(i,j) = 1$ if zone (node) i is connected to zone (node) j, otherwise $\boldsymbol{C_M}(i,j) = 0$
  - maximum capacity of each transmission line ($\boldsymbol{T_C}$)

2.2 Power Sector Simulation

2.2.1 Pre-Processing

Demand and Generation profiles

The hourly (h) electric load profiles of each zone z are stored in the matrix $\boldsymbol{D(h,z)}$, and are obtained by scaling the demand profile of the reference year according to the formula:

$$\boldsymbol{D(h,z)} = D_{z\,tot} \cdot \frac{\boldsymbol{D_{ref}}(h,z)}{\sum_h \boldsymbol{D_{ref}}(h,z)} \tag{2.2.1}$$

where $\boldsymbol{D_{ref}}(h,z)$ is the reference demand profile of hour h for zone z.
The possible Import/Export profile is computed in the same way.
Similarly, the generation profile $\boldsymbol{G_i}$ of the i-th technology belonging to "type 1" is defined as:

$$\boldsymbol{G_i}(h,z) = Pn_{i,z} \cdot e_{h_{i,Z}} \cdot \frac{\boldsymbol{G_{i\,ref}}(h,z)}{\sum_h \boldsymbol{G_{i\,ref}}(h,z)} \tag{2.2.2}$$

A simple example is shown in figure 2.1, where the 2050 on-shore wind power profile of Sardinia, supposing $Pn_{2050} = 2.5\,GW$ and $e_h = 2400$ is computed starting from the 2017 profile, $Pn_{2017} = 1\,GW$ (Terna data). If the copper-plate approach is used, the profiles of the different zones are summed into a single vector.

Finally, all the profiles of the "type 1" technologies are added together, obtaining the "Base and Must-run" (*BMR)* profile. To this category belong all those plants whose power output is assumed to be fixed: typically these include base-load plants with low flexibility and renewable source plants, which are assumed to have dispatch priority since they are characterized by low marginal cost and do not emit greenhouse gases.

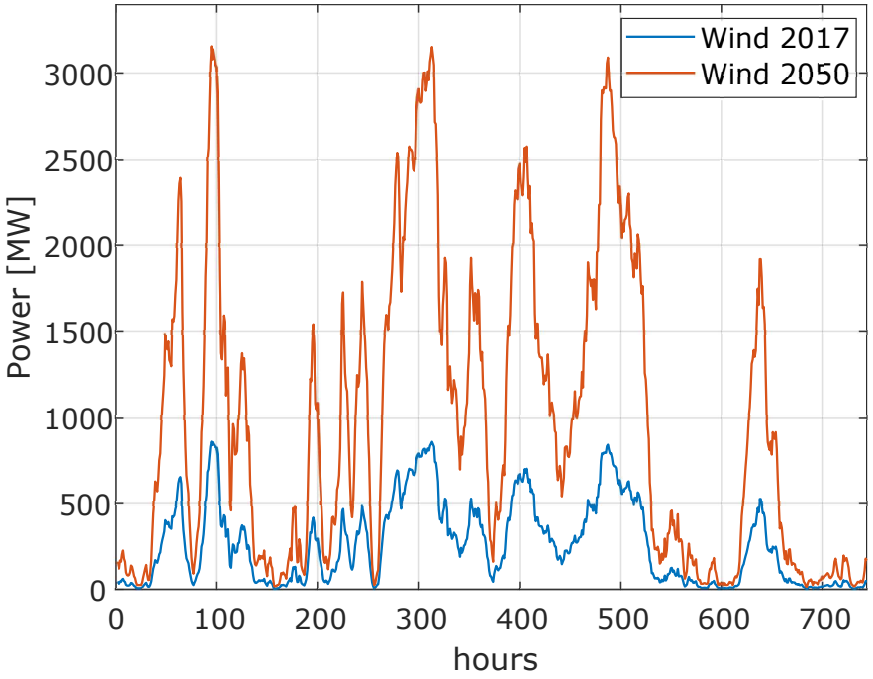

Figure 2.1: 2050 and 2017 wind generation profile of Sardinia. Only January data are shown.

Estimation of Limited-Dispatchable-Energy Exploitability

As mentioned earlier, in COMESE two categories of flexible generators for dispatch management are distinguished: the first includes water-reservoir hydropower plants (*HyDam*), which, for each zone, have a maximum annual deliverable energy; the second includes fuel-fired plants, which do not have this limitation (actually, an energy limit can be defined for them as well, e.g., associated with biogas availability, but, in this case, the constraint is national and not zonal since it is assumed that fuel transport can take place without any limitation). It is therefore important to consider how to distribute the usable energy so that it is available throughout the year during periods of high residual demand. So a curve is created whose integral is equal to the total available energy during a year (8760 hours) and whose amplitude is a rough estimate of the unserved demand after the exploitation of the Base&Must-Run (*BMR*) generators and storage plants.

Specifically, for each zone, first the BMR generation is compared to the demand in order to identify deficit and surplus hours. From that, the contribution of storage plants is estimated so as to obtain the residual demand curve. Then the the time frame under investigation is divided into a number of intervals equal to N_h/N_{LTFW} and $\boldsymbol{E_{disp\,tot}}(z)$

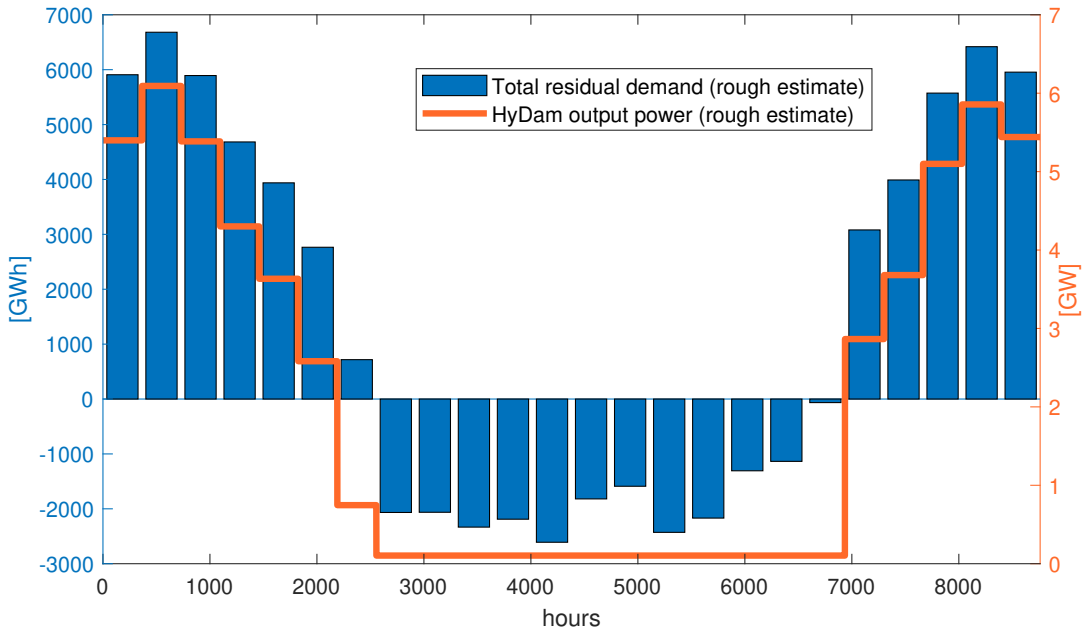

Figure 2.2: Available energy allocation of *Hydam* plants, nord zone, 2050 Scenario. The analysis time frame (one year) is divided into 24 intervals of 365 hours each. The integral of the orange curve is equal to $E_{disp\,tot}$

is distributed according to the share of total residual demand of each interval. As can be seen in figure 2.2, during the intervals with negative total residual demand (when the energy produced by *BMR* and storage plants is assumed to be greater than the energy demanded by the load), the estimated *HyDam* output power is set to a small but non-zero value, while the maximum value of the curve is limited to P_n.

Incidence Matrix

Starting from $\boldsymbol{C_M}$ it is possible to compute the transmission matrix (or incidence matrix) $\boldsymbol{M_T}$, which sorts the connection from the first one to the last one (giving them a univocal order). For each transmission line (column) the starting node is identified with "-1" and the ending note with "+1", where the current conventional direction is from the lower-index zone to higher-index zone. So dimensions of $\boldsymbol{M_T}$ are $N_Z \times N_I$ where N_I is the total number of interconnections between the zones. For instance, considering

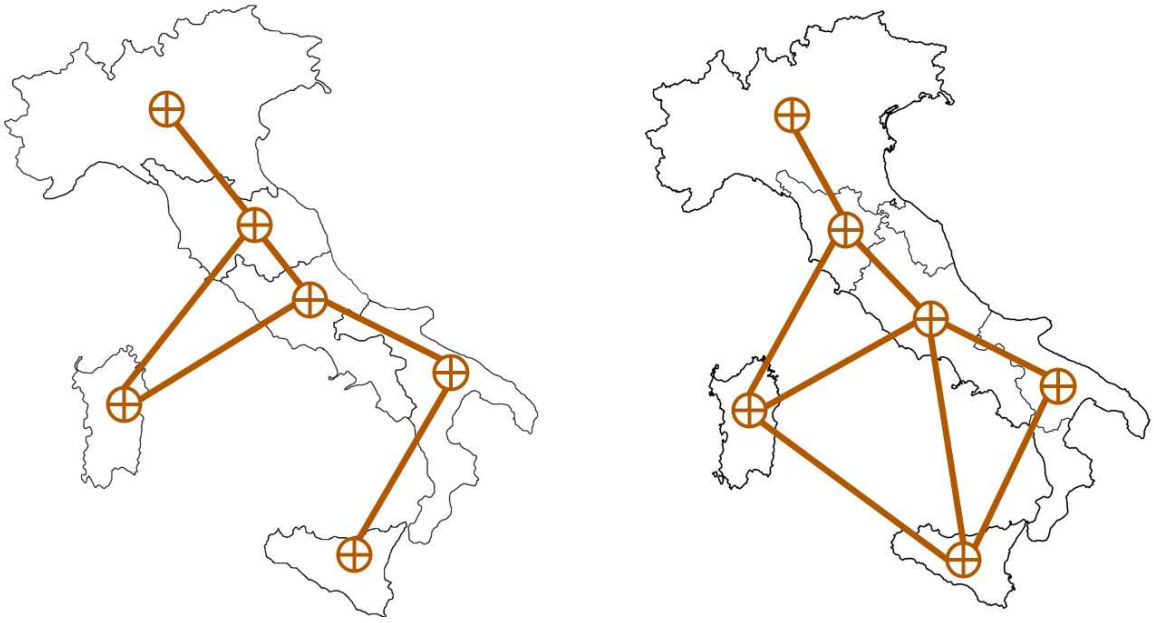

Figure 2.3: Representation of Italian transmission gird: model currently used in the electric market (left) and evolution according to *Piano di Sviluppo 2021* (right).

the grid model currently used in the Italian electricity market (figure 2.3) we get:

$$\boldsymbol{C_M} = \begin{bmatrix} 0 & 1 & 0 & 0 & 0 & 0 \\ 1 & 0 & 1 & 0 & 0 & 1 \\ 0 & 1 & 0 & 1 & 0 & 1 \\ 0 & 0 & 1 & 0 & 1 & 0 \\ 0 & 0 & 0 & 1 & 0 & 0 \\ 0 & 1 & 1 & 0 & 0 & 0 \end{bmatrix}, \quad \boldsymbol{M_T} = \begin{bmatrix} -1 & 0 & 0 & 0 & 0 & 0 \\ 1 & -1 & -1 & 0 & 0 & 0 \\ 0 & 1 & 0 & -1 & -1 & 0 \\ 0 & 0 & 0 & 1 & 0 & -1 \\ 0 & 0 & 0 & 0 & 0 & 1 \\ 0 & 0 & 1 & 0 & 1 & 0 \end{bmatrix}$$

whereas, if the expansion planned by Terna in [23] is considered:

$$\boldsymbol{C_M} = \begin{bmatrix} 0 & 1 & 0 & 0 & 0 & 0 \\ 1 & 0 & 1 & 0 & 0 & 1 \\ 0 & 1 & 0 & 1 & 1 & 1 \\ 0 & 0 & 1 & 0 & 1 & 0 \\ 0 & 0 & 0 & 1 & 0 & 1 \\ 0 & 1 & 1 & 0 & 1 & 0 \end{bmatrix}, \quad \boldsymbol{M_T} = \begin{bmatrix} -1 & 0 & 0 & 0 & 0 & 0 & 0 & 0 \\ 1 & -1 & -1 & 0 & 0 & 0 & 0 & 0 \\ 0 & 1 & 0 & -1 & -1 & -1 & 0 & 0 \\ 0 & 0 & 0 & 1 & 0 & 0 & -1 & 0 \\ 0 & 0 & 0 & 0 & 1 & 0 & 1 & -1 \\ 0 & 0 & 1 & 0 & 0 & 1 & 0 & 1 \end{bmatrix}$$

The power flow analysis is carried out in a simplified way: transmission lines are represented as simple connections that allow the exchange of active power between zones within line capacity limits. Therefore this model ignores the effects of node voltage and line impedance on flows (including losses) and, besides the capacity constraint, only requires nodal power balance [20].

Mathematical formulation of dispatchment

The code performs an hourly simulation of the power sector and, for each hour of the year, the operation of the various technologies is optimized in order to meet the demand. Mathematically, this corresponds to solving a linear least-squares system with bounds and linear constraints in the form:

$$\min_{x}\left\{\frac{1}{2}\|\boldsymbol{C}\cdot\boldsymbol{x}-\boldsymbol{d}\|_2^2\right\} \text{ such that } \begin{cases}\boldsymbol{A}\cdot\boldsymbol{x}\leq\boldsymbol{b}\\ \boldsymbol{A_{eq}}\cdot\boldsymbol{x}=\boldsymbol{b_{eq}}\\ \boldsymbol{l_b}\leq\boldsymbol{x}\leq\boldsymbol{u_b}\end{cases} \tag{2.2.3}$$

MATLAB provides the "lsqlin" function to solve this problem, so during the thesis work (see chapter 3) it was studied whether there are better alternatives and which solver options best fit the overall code structure, so to balance solution accuracy and computation time. The next section quickly presents how the system of equations (2.2.3) is applied for the management of the various technologies in the original version of COMESE.

2.2.2 Hourly System Operation

For each hour of the year, the code attempts to satisfy the power balance between demand and net generation using the following fixed order of commitment for the various technologies:

1. *BMR* generators;
2. storage plants;
3. *HyDam* plants;
4. natural gas-fired dispatchable power plants

If then there is still some unserved load, the "mid-analysis" section comes into play. The various sections work sequentially: each determines the operation of the technology

under analysis (based on the outputs of the previous sections). The generation mix that meets demand at a given time is determined only as last step.

Baseload&Must-Run plants

Referring to system (2.2.3), $\boldsymbol{x}$ is the vector containing the variables associated both with the power flows on the lines (which are bounded within the transmission capacity values), and with the *BMR* power used to meet the load in each zone (which is bounded between 0 and the *BMR* generation in that zone). Therefore, for hour h, if we consider of not having forecast interval it holds:

$$\boldsymbol{x_h} = \begin{pmatrix} \boldsymbol{PF_{BMR}}(h,1) \\ \vdots \\ \boldsymbol{PF_{BMR}}(h,N_I) \\ \boldsymbol{P_{BMR}}(h,1) \\ \vdots \\ \boldsymbol{P_{BMR}}(h,N_Z) \end{pmatrix} \quad \boldsymbol{l_{b_h}} = \begin{pmatrix} -\boldsymbol{T_C}(1) \\ \vdots \\ -\boldsymbol{T_C}(N_I) \\ 0 \\ \vdots \\ 0 \end{pmatrix} \quad \boldsymbol{u_{b_h}} = \begin{pmatrix} \boldsymbol{T_C}(1) \\ \vdots \\ \boldsymbol{T_C}(N_I) \\ \boldsymbol{G_{BMR}}(h,1) \\ \vdots \\ \boldsymbol{G_{BMR}}(h,N_Z) \end{pmatrix} \tag{2.2.4}$$

The term $\boldsymbol{C} \cdot \boldsymbol{x}$ corresponds to the net power available in each zone, including the net imported energy from other regions. $\boldsymbol{d}$ represent the zonal demand:

$$\boldsymbol{C} = \boldsymbol{C_h} = \begin{bmatrix} \boldsymbol{M_T} & \boldsymbol{I_{N_Z \times N_Z}} \end{bmatrix} \tag{2.2.5}$$

where $\boldsymbol{I_{N_Z \times N_Z}}$ is the identity matrix of dimensions $N_Z \times N_Z$, and

$$\boldsymbol{d} = \boldsymbol{d_h} = \begin{pmatrix} \boldsymbol{D}(h,1) \\ \vdots \\ \boldsymbol{D}(h,N_Z) \end{pmatrix} \tag{2.2.6}$$

So the solver minimizes in the least-square sense the residual demand $\boldsymbol{R} = \boldsymbol{C} \cdot \boldsymbol{x} - \boldsymbol{d}$. Actually, in this way priority is given to zones with high demand, as their contribution to the norm of the residual has a greater weight (see figure 2.4). Consequently, $\boldsymbol{C}$ and $\boldsymbol{d}$ are multiplied (element-wise) by the coefficient $\boldsymbol{K_D}$ in order to normalize the zones

to the total demand:

$$\boldsymbol{K_D}(z) = \boldsymbol{K_{D_h}}(z) = \frac{\sum_{z=1}^{N_Z} \boldsymbol{D}(h,z)}{\boldsymbol{D}(h,z)} \tag{2.2.7}$$

If $h_{FW} \geq 1$ the code "looks into the future" (the usefulness of this feature is better explained in the storage section), therefore the system of equations (2.2.3) must take into account also the quantities related to the h_{FW} hours ahead. $\boldsymbol{C}$ is build by "placing" $h_{FW}+1$ times $\boldsymbol{C_1}$ along its diagonal (obtaining a matrix of dimensions $[N_Z \cdot (h_{FW}+1)] \times [(N_I+N_Z)\cdot(h_{FW}+1)]$), whereas $\boldsymbol{d}$, $\boldsymbol{K_D}$, $\boldsymbol{l_b}$, $\boldsymbol{u_b}$ include the all the terms also of the hours up to $h + h_{FW}$:

$$\boldsymbol{C} = \begin{bmatrix} \boldsymbol{C_h} & & \\ & \boldsymbol{C_h} & \\ & & \ddots \end{bmatrix} \quad \boldsymbol{d} = \begin{pmatrix} \boldsymbol{d_h} \\ \vdots \\ \boldsymbol{d_{h+h_{FW}}} \end{pmatrix} \quad \boldsymbol{u_b} = \begin{pmatrix} \boldsymbol{u_{b_h}} \\ \vdots \\ \boldsymbol{u_{b_{h+h_{FW}}}} \end{pmatrix} \quad \boldsymbol{l_b} = \begin{pmatrix} \boldsymbol{l_{b_h}} \\ \vdots \\ \boldsymbol{l_{b_{h+h_{FW}}}} \end{pmatrix} \tag{2.2.8}$$

$\boldsymbol{A}$ is set equal to $-\boldsymbol{C}$ and $\boldsymbol{b}$ to 0, so as to impose, for each zone, that the power export cannot exceed the sum of the generated import power. Finally, for each hours within the forecast interval, the outputs of this section are:

- zonal residual demand or deficit ($\mathbf{Def_1}$)
- zonal power surplus (**Surp**). It is obtained by subtracting the actual exploited *BMR* power from the *BMR* generation profile.
- power flows due to *BMR* exploitation ($\boldsymbol{PF} = \boldsymbol{PF}_{BMR}$).

.

Storage plants

Storage charge can occur only during non-defict hours and it is performed using again *lsqlin*: storage plants are seen as loads and the solver tries to minimize $\boldsymbol{Surp}$. So, if two storage technologies are taken into account (for instance Hydro Pumped Storage and Electrochemical Storage), then:

$$\boldsymbol{C_h} = \begin{bmatrix} \boldsymbol{M_T} & -\boldsymbol{I_Z} & -\boldsymbol{I_Z} \end{bmatrix}, \quad \boldsymbol{d_h} = \begin{pmatrix} -\boldsymbol{Surp}(h,1) \\ \vdots \\ -\boldsymbol{Surp}(h,z) \end{pmatrix} \tag{2.2.9}$$

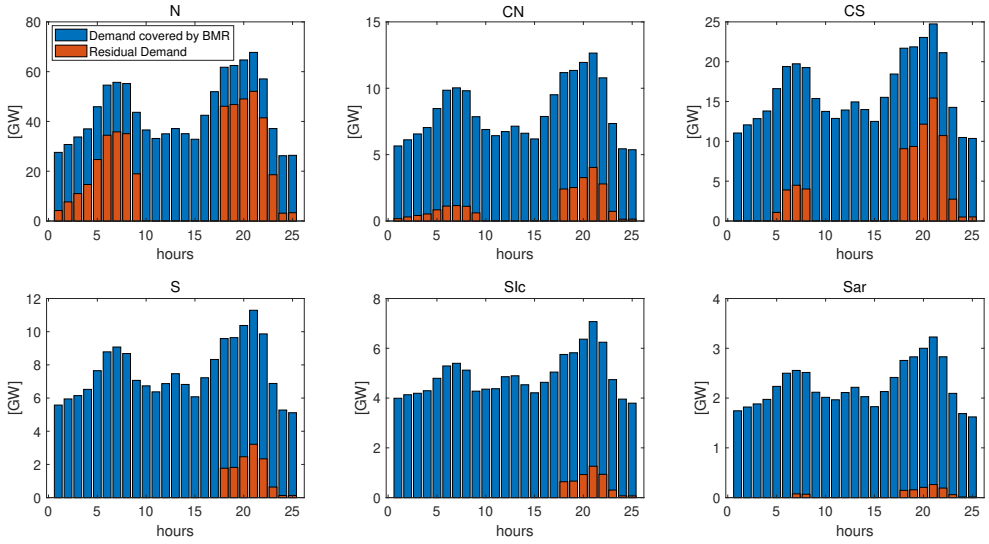

(a) 6 zones, 24 hours, *BMR* exploitation with $\boldsymbol{K_D}$

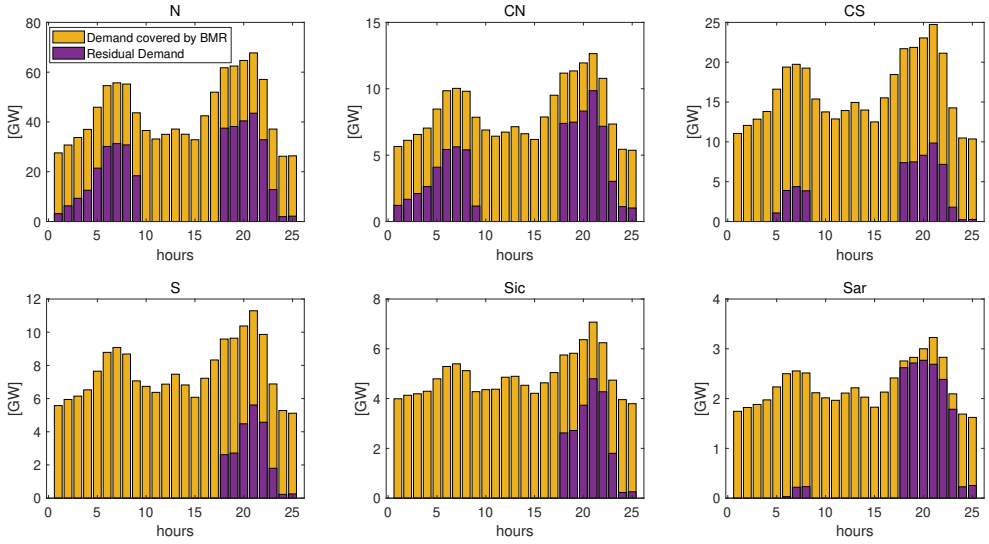

(b) 6 zones, 24 hours, *BMR* exploitation without $\boldsymbol{K_D}$

Figure 2.4: Effect of K_D coefficient: without K_D (bottom figure), the zones with low demand are penalized, and have high relative values of residual demand with respect to the case with K_D (upper figure).

and $\boldsymbol{C}$ and $\boldsymbol{d}$ are computed as in (2.2.8). Considering a storage plant of type s in zone z, its input power is limited between 0 and $Pn_{stor}(s,z)$. Since each section works independently, the constraints on the variables associated with the power flows must also include the outcomes of the power flows resulting from the previous sections $\boldsymbol{PF}_{former}$ (in this case they are equal to $\boldsymbol{PF}_{BMR}$) . Therefore, for a generic line I, the available transmission capacity is updated to $\boldsymbol{T_C}(I) - \boldsymbol{PF}_{former}(I)$. Compared to the *BMR* case, $\boldsymbol{A}$ and $\boldsymbol{b}$ must include constraints on the maximum energy that can be stored: for each possible charging interval within the forecast interval, the total stored energy (considering the charging efficiency) cannot exceed the maximum capacity of the plant.

If storage plants are fully charged and there is still excess energy available, *lsqlin* tries to distribute it evenly among the zones so as to reduce the norm of the residual. Consequently, a post-processing section is needed so that dummy loads take the excess surplus in the various zones, thus avoiding unnecessary power flows.

Storage discharge can only occur during "deficit hours", i.e. hours characterized by the presence of unserved demand. In this way it is ensured that, for each hour, any storage system can either discharge or charge, and power flows due to charging do not affect those due to discharging. Anyway, the approach is similar to that used for *BMR* technologies, where the demand $\boldsymbol{D}$ is replaced by the residual deficit $\mathbf{Def_1}$, again weighted with $\boldsymbol{K_D}$:

$$\boldsymbol{C_h} = \begin{bmatrix} \boldsymbol{M_T} & \boldsymbol{I_Z} & \boldsymbol{I_{N_Z \times N_Z}} \end{bmatrix}, \quad \boldsymbol{d_h} = \begin{pmatrix} \boldsymbol{Def_1}(h,1) \\ \vdots \\ \boldsymbol{Def_1}(h,z) \end{pmatrix} \tag{2.2.10}$$

The discharge management is strongly influenced by the length of the forecast interval: in fact, not only the output power is limited to Pn_{stor}, but the maximum energy that can be delivered by storage systems cannot exceed that stored during the previous charging hours (again, this constraint is included in $\boldsymbol{A}$ and $\boldsymbol{b}$). Consequently, if the solver knows the charging and $\mathbf{Def_1}$ profiles for a certain number of hours, it can distribute the available energy "wisely" during the various hours of discharge. To better explain this concept, let's consider a single zone and the residual demand profile of figure 2.5a. If $h_{FW} = 0$, each hour is treated separately and storage is completely discharged within the first four hours (figure 2.5b), whereas if $h_{FW} = 20$, the same amount of

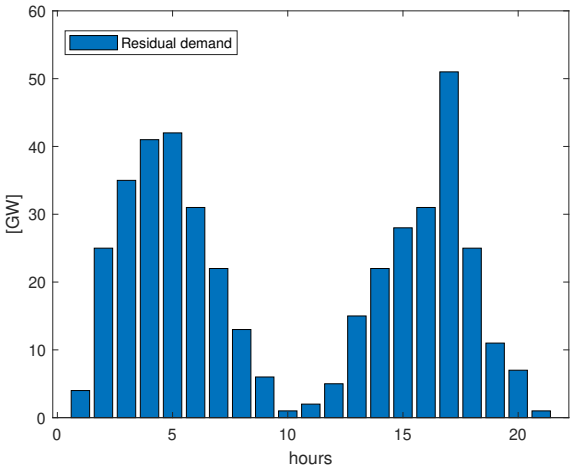

(a) Residual demand profile after *BMR* exploitation

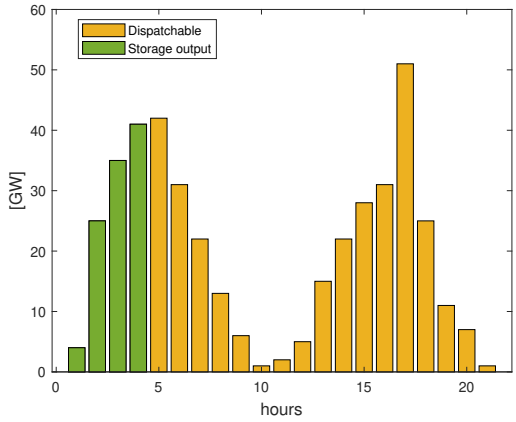

(b) Storage discharge, without forecast interval

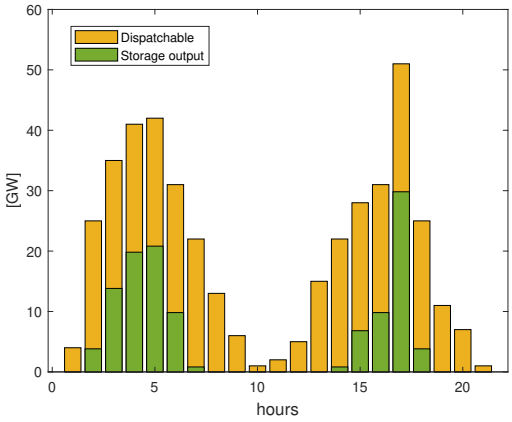

(c) Storage discharge, with forecast interval

Figure 2.5: Effect of forecast interval on storage discharge and dispatchable generation

energy is delivered optimally, in the sense of equation (2.2.3), increasing storage output during peak-load hours (see figure 2.5c). This also strongly influences the behavior of dispatchable generation: in the former case *HyDam* and turbo-gas plants have to cover a very fluctuating residual load, and it might happen that the nominal power of these plants is not enough to cover the demand at peak hours. In the latter case the power they should provide is more uniform and stays at lower values thus reducing the rated power of dispatchable generators needed to ensure demand balancing.
To summarize, after performing charging, post-processing, and discharging, the outputs of this section are:

- charging (or input) and discharging (or output) power profile of storage plants, respectively $\boldsymbol{Pch_s}$ $\boldsymbol{Pdch_s}$
- zonal residual demand or deficit $\mathbf{Def_2}$

- zonal residual surplus, i.e. residual excess generation (or overgeneration) by *BMR* $\boldsymbol{P_{OG}}$.
- power flows due to storage plants operation $\boldsymbol{PF_{stor}}$ and updated net power flows $\boldsymbol{PF = PF_{stor} + PF_{former}}$.

Energy-constrained dispatchable plants

Energy-constrained dispatchable plants include *HyDam* plants and, as explained in section (2.2.1), the energy they can deliver in a year is limited, for each zone, to a maximum value $\boldsymbol{E_{disp\,tot}}(z)$. For each hour of the year, the available energy over the entire forecast interval is computed as

$$\boldsymbol{E_{HyDam}(z)} = \sum_{i=h}^{i=h+h_{FW}} P_{est_{Hy}}(i,z) \tag{2.2.11}$$

where $P_{est_{Hy}}$ is the estimated output power obtained from the curve of figure 2.2. $\boldsymbol{A}$ and $\boldsymbol{b}$ are again used to impose that

$$\sum_{i=h}^{i=h+h_{FW}} \boldsymbol{P_{HyDam}}(i,z) \leq \boldsymbol{E_{HyDam}}(z) \tag{2.2.12}$$

where $\boldsymbol{P_{HyDam}}(i,z)$ is the power generated by hydro water reservoir plants in zone z during hours i. The remaining constraints are defined as in the previous sections, and *HyDam* generation is used to cover the residual demand $\mathbf{Def_2}$. The final outputs are:

- *HyDam* generation profile $\boldsymbol{P_{HyDam}}$
- zonal residual demand or deficit $\mathbf{Def_3}$
- power flows due to *HyDam* plants operation $\boldsymbol{PF_{HyDam}}$ and updated net power flows $\boldsymbol{PF = PF_{HyDam} + PF_{former}}$

Energy-unconstrained dispatchable plants

Fuel-fired dispatchable generators are the last plants called to come into operation (if unserved demand is still present), since this category includes turbo-gas generators, which are characterized by high marginal cost and emit CO_2 emissions, whether they are fueled by natural gas or bio-gas. These plants are managed in the same way as *HyDam* plants: the only difference is that now $E_{disp\,tot}$ is a single global value, i.e.

no distinction is made among zones. So the available energy over the entire forecast interval is

$$E_{Gas} = \sum_{i=h}^{i=h+h_{FW}} P_{est_{Gas}}(i) \tag{2.2.13}$$

leading to the constraint

$$\sum_{z=1}^{z=N_Z} \sum_{i=h}^{i=h+h_{FW}} \boldsymbol{P_{Gas}}(i,z) \leq E_{Gas} \tag{2.2.14}$$

The outputs of this section are:

- Turbo-gas generation profile $\boldsymbol{P_{Gas}}$
- Zonal residual demand or unserved load $\mathbf{Def_4}$
- Power flows due to turbo-gas plants operation $\boldsymbol{PF_{Gas}}$ and updated net power flows $\boldsymbol{PF} = \boldsymbol{PF_{Gas}} + \boldsymbol{PF_{former}}$

Mid-Analysis

Perfect forecast is assumed, that is the analyses in each section (BMR, Storage,etc) described above are based on the perfect knowledge of generation and demand in the whole time interval, i.e. for hour h, to $h + h_{FW}$. Therefore, the code determines the generation mix that satisfies the demand for all the hours within the forecast interval. For example figure 2.6 shows how the different technologies and the power exchanges between the zones $\boldsymbol{Exc}$[1] contribute to meet the demand in a system with high penetration of RES and storage. However if there are still unserved load hours within the forecast interval COMESE adjusts the system management during the current hour h, further exploiting storage plants and dispatchable generators. In particular the following steps are carried out:

1. If hour h is a "deficit hour", storage technologies are further discharged (within power and capacity limits) in order to try to meet the load.
2. if dispatchable generators (both *HyDam* and turbo-gas) are not working at their maximum power, they are used to reduce the storage output of hour h, so that more energy will be available during the following deficit hours.

[1] $\boldsymbol{Exc} = \boldsymbol{M_T}' \cdot \boldsymbol{PF}$

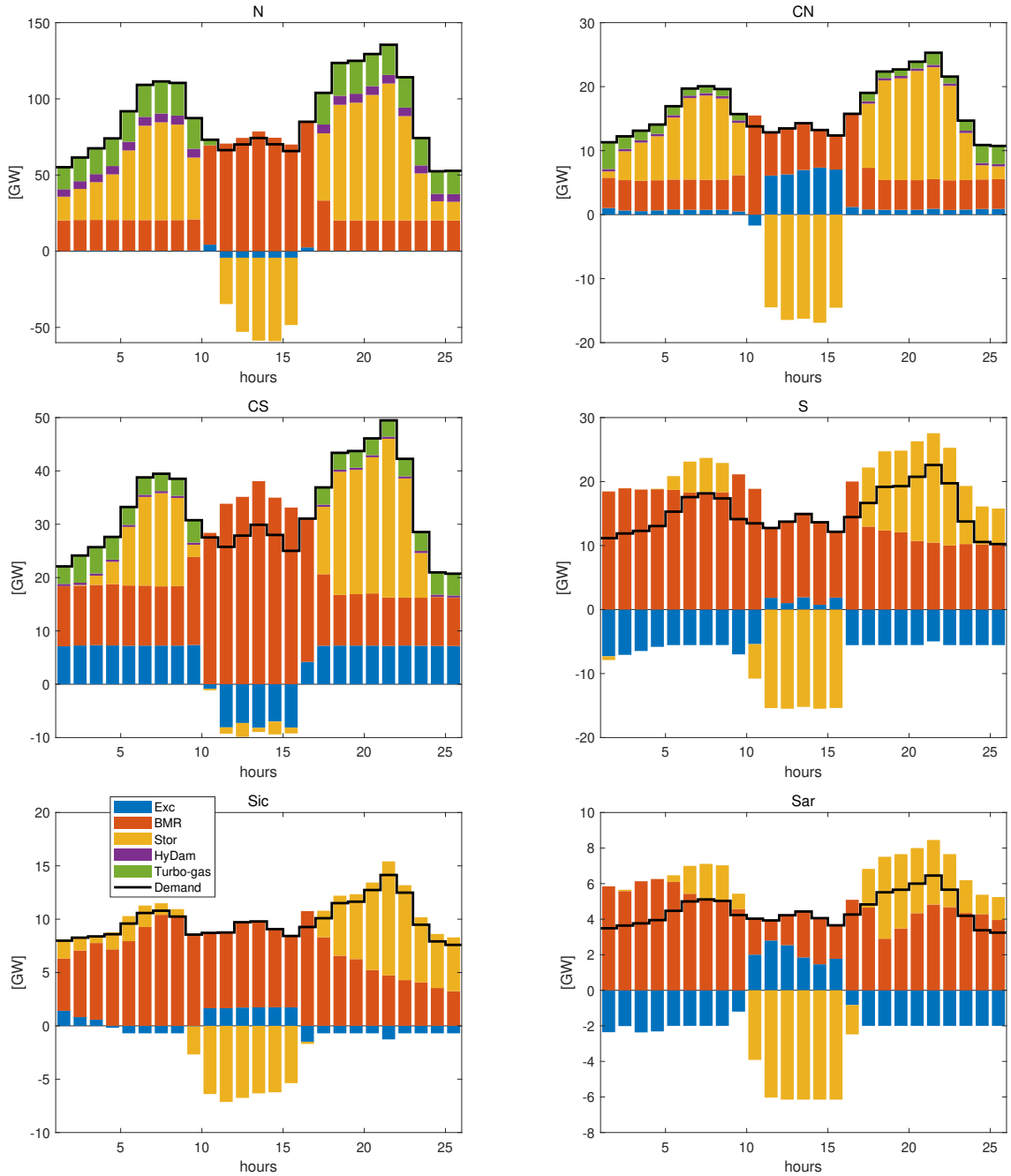

Figure 2.6: Power system hourly operation within a forecast interval, per each of the 6 zones, electricity market grid model

3. if dispatchable generators (both *HyDam* and turbo-gas) are not working at their maximum power, they are used to charge storage plants, delivering an amount of energy equal to the total unmet load expected in the following h_{FW} hours (obviously all the constraints explained in the previous section must be respected).

In this way dispatchable power plants are extensively exploited only if it is strictly needed in order to meet the load.
At this point, the electricity generation mix used to meet the demand is defined, as well as the possible share of unserved load, and the following hour *h+1* is studied starting again from the *BMR* section.

2.3 LCOTE computation

Once the hourly operation of the system has been simulated, the last section of COMESE involves the calculation of the average discounted cost of electricity for the scenario considered. This average cost is named LCOTE (Levelized Cost of Timely Electricity) where "Timely" specifies that the data obtained and used to calculate the cost take into account the actual hourly operation of the system.
Provided that N_p different kinds of power plants are generating electricity and N_s storage technologies are involved, the LCOTE is calculated as follows:

$$LCOTE = \frac{\sum_{i=1}^{i=N_p} (LCOE_i \cdot E_i) + Co_{stor}}{E_{load}} \tag{2.3.1}$$

where $LCOE_i$ is the well known levelized lifetime average cost of electricity generated by the ith technology, E_i and E_{load} are the electricity generated by the ith technology and the annual electricity demand, respectively. Co_{stor} is the annual cost of energy storage systems, which is computed as follows:

$$Co_{stor} = \sum_{j=1}^{j=N_s} I_j \frac{r(1+r)^{n_j}}{(1+r)^{n_j} - 1} + O\&M_j \tag{2.3.2}$$

where I_j is the investment costs of the j-th storage technology (usually pumped-hydro or batteries), $O\&M_j$ its annual average operation and maintenance costs, n_j its expected lifetime and r the lifetime average discount rate. Therefore, unlike LCOE, LCOTE is a parameter concerning the whole electricity system that represents the average cost per

year of a kWh generated and consumed, taking into account the costs of all technologies required to ensure the availability of electric power 24 hours a day. In addition to the deterministic approach, COMESE can perform an economic analysis with a stochastic approach based on the Monte Carlo method: in this case parameters such as investment and O&M costs, fuel cost and lifetime are varied within a chosen range following an assigned probability distribution so to estimate a probability distribution for the LCOTE. This approach is particularly useful given the difficulty in establishing an unambiguous value for future factor of cost of a technology, especially the uncertainties on the scenario considered increases.

2.4 Power System Optimization

In the case of deterministic economic analysis, it is possible to carry out an optimization process of the power system configuration, using the LCOTE parameter as the objective function, so as to identify the installed capacity of various technologies that, under given conditions and with imposed constraints, results in the lowest electricity cost. The optimizer is based on the Differential Evolution (DE) algorithm, a metaheuristic technique particularly suitable, in terms of efficiency and robustness, for the solution of problems characterized by non-differentiable objective functions and potentially high computational costs [26]; here it is extended to allow also the study of constrained optimization problems [18]. In particular, after setting the DE parameters such as the population size, mutation and crossover ratio and the maximum number of iterations, the user can decide on a number of variables to be made to vary continuously within a certain range, for example, the installed capacity of PV, storage, and turbo-gas generators in a reference scenario. So the algorithm generates a first population of candidate solutions by choosing randomly the values of these variables and running the simulation of the resulting power systems as explained in section 2.2.2. A solution is considered feasible if it satisfies given constraints, such as the maximum allowed number of hours of unmet load and the maximum energy produced by dispatchable generators. An "offspring" population is then created by mutation and cross-over of the "parents" variables; the new set of candidate solutions is defined by choosing among the "more feasible" individuals the ones that best fit the optimization problem, i.e. that have the lowest LCOTE. The process is repeated iteractively until the maximum number of iterations (generations) is reached (figure 2.7).

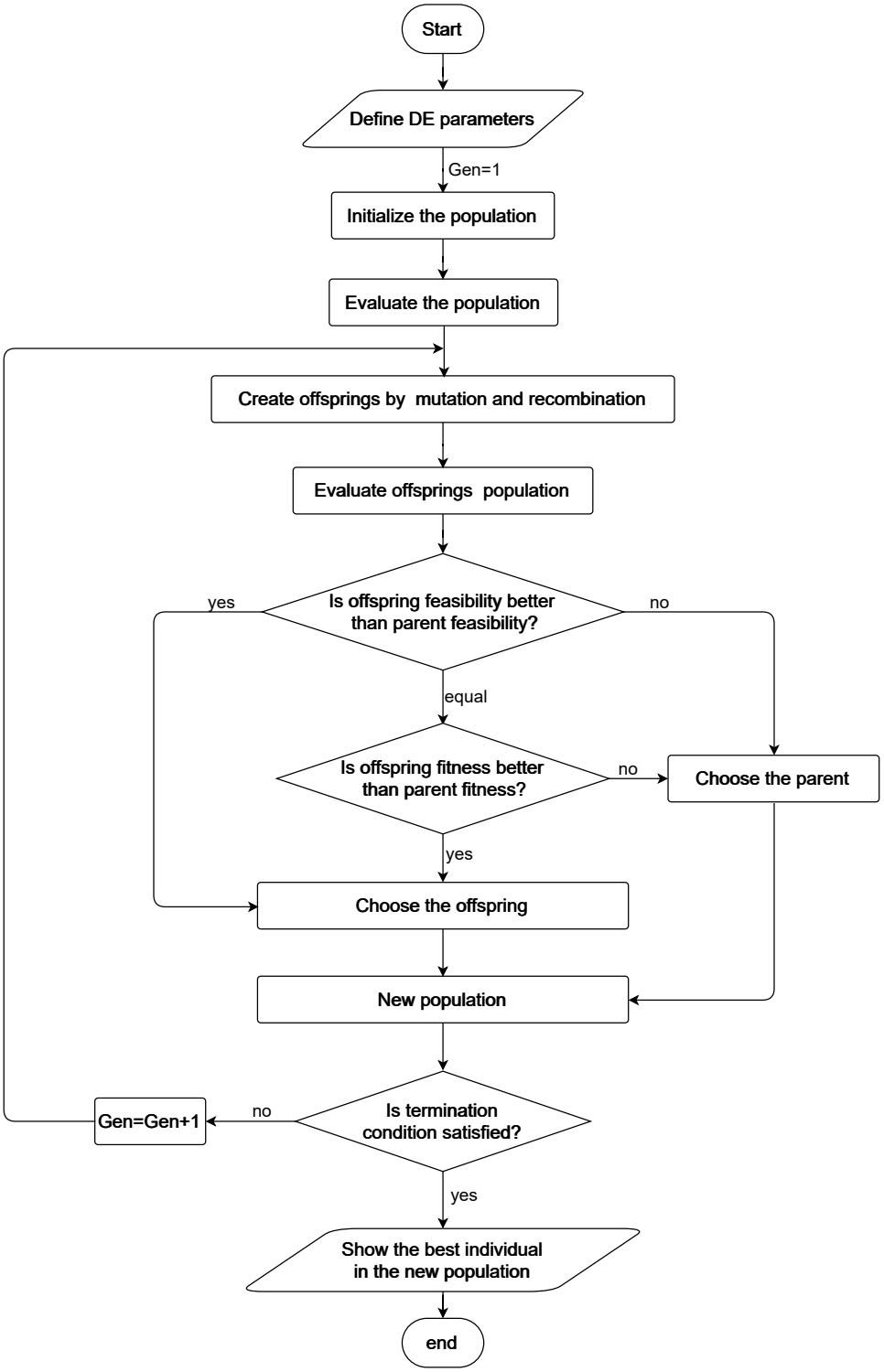

Figure 2.7: Differential evolution algorithm

Chapter 3

Improvements introduced in COMESE

This chapter presents the main upgrades made to COMESE. The work is focused on enhancing the zonal model of the power sector, but particular attention was also paid to the computational burden. In this sense, several modifications are presented as alternatives that can be selected according to the user's needs, so as to obtain a robust and versatile tool, adaptable to various kinds of analysis.

The first section deals with the transmission grid model and power flows computation. In particular two approaches are presented and validated that give the possibility to minimize power exchanges between zones without affecting the system cost and the demand coverage. Then line power losses are introduced using a simplified linear description.

The modifications on the storage model are presented in the second section. They concern both on the charge and discharge operation and, again, multiple alternatives have been implemented either to increase the computational speed of the code, or to improve the degree of detail in the management of storage technologies.

The results from the previous sections suggested that it was possible to simplify the mathematical model used to ensure optimal meeting of the demand (see paragraph 2.2.2). In particular, in the last part of this chapter, it is shown that, in some cases, it is not necessary to solve a linear least-squares system, but is sufficient to find the minimum of a linear function, thus drastically reducing the computational burden (without significantly affecting the LCOTE).

Finally, an economic characterization of the transmission grid is introduced. This gives the possibility to perform optimization analysis aimed at identifying the trade-off between additional interconnection capacity and generation capacity, so as to minimize the total system costs.

3.1 Power Flow model

As explained in chapter 2, with the introduction of transmission lines the $\boldsymbol{C}$ matrix in the system of equations (2.2.3) becomes rectangular: in general its dimensions are $[N_Z \cdot (h_{FW} + 1)] \times [(N_I + N_Z \cdot N_t) \cdot (h_{FW} + 1)]$ where N_t is the number of "alternatives" of a certain technology (for instance in the storage section Hydro Pumped Storage and Electrochemical Storage are taken into account, but one could decide to adopt a more precise distinction even in the other COMESE sections). This leads to the fact that, in certain conditions, the system (eq. 2.2.3) does not have a unique solution, i.e. the load of each zone can be covered by an infinite number of combinations of power generated in the various zones and power flows along the lines (see appendix A.1 for a more precise explanation).
It is therefore important to define what the purpose of the analysis is: if the user's focuses is on the final main final outcomes, such as hours of unserved load and LCOTE, in order to to assess the feasibility of a given scenario, he/she might not be interested in which of the possible solutions (that lead to the same macroscopic results) has been selected; in this case, the grid acts only as a constraint and it is not important to analyse the hourly and zonal behaviour of each power plant and transmission line. On the other hand, it might be useful to choose a precise rationale of grid management and study the response of the system under this particular assumption, which, however, should not affect the ability to meet the demand; in this case, among all the possible solutions, it is necessary to identify the desired one, otherwise the MATLAB solver provides a result over which the user has no control.
In this work, two approaches are shown that allow obtaining a solution where the grid power flows are minimized.

3.1.1 Power Flows minimization

Post-processing approach

This approach maintains unchanged the original version of the various sections of the code, but after each intermediate step, i.e. after each call of *lsqlin*, a post-processing section is added to "adjust" the results just obtained.
Consider for example the *BMR* section: let's call $\boldsymbol{x_1}$ the solution obtained solving system of eq. (2.2.3), see section 2.2.2 for the description of the parameters. As said above, the minimization of the power flows should not impact on demand coverage, therefore

the solution resulting from the post-processing ($\boldsymbol{x_{pp}}$) must keep the residual demand unchanged obtained with $\boldsymbol{x_1}$, mathematically:

$$\boldsymbol{R} = \boldsymbol{C} \cdot \boldsymbol{x_1} - \boldsymbol{d} = \boldsymbol{C} \cdot \boldsymbol{x_{pp}} - \boldsymbol{d} \tag{3.1.1}$$

So the equality constraints for the post-processing are built as follow:

$$\boldsymbol{A_{eq,pp}} = \begin{bmatrix} \boldsymbol{A_{eq}} \\ \boldsymbol{C} \end{bmatrix}, \qquad \boldsymbol{b_{eq,pp}} = \begin{pmatrix} \boldsymbol{b_{eq}} \\ \boldsymbol{R} + \boldsymbol{d} \end{pmatrix} \tag{3.1.2}$$

All the other bounds and constraints are equal to the ones used to get $\boldsymbol{x_1}$. As regards $\boldsymbol{C_{pp}}$ and $\boldsymbol{d_{pp}}$, the goal is to minimize the power exchanges between the zones: in order to obtain, at the end of each section, net power flows as close as possible to zero, it is necessary that the power flows resulting from exploitation of the technology under analysis (*BMR*, Storage, *HyDam*,...) are set equal to the opposite of the power flows resulting from the previous sections ($\boldsymbol{PF} = \boldsymbol{PF}_{\text{"section"}} + \boldsymbol{PF_{former}}$). In this way the solver has the possibility to "freeze" partial power flows obtained in the previous sections. So, if a single hour h is considered:

$$\boldsymbol{C_{pp,h}} = \begin{bmatrix} \boldsymbol{I}_{N_I \times N_I} & \\ & \boldsymbol{0}_{N_Z \times N_Z} \end{bmatrix} \qquad \boldsymbol{d_{pp,h}} = \begin{pmatrix} -\boldsymbol{PF_{former}}(h,1) \\ \vdots \\ -\boldsymbol{PF_{former}}(h,N_I) \\ \boldsymbol{0}_{N_Z \times 1} \end{pmatrix} \tag{3.1.3}$$

or, if the zero-rows are removed

$$\boldsymbol{C_{pp,h}} = \begin{bmatrix} \boldsymbol{I}_{N_I \times N_I} & \boldsymbol{0}_{N_I \times N_Z} \end{bmatrix} \qquad \boldsymbol{d_{pp,h}} = \begin{pmatrix} -\boldsymbol{PF_{former}}(h,1) \\ \vdots \\ -\boldsymbol{PF_{former}}(h,N_I) \end{pmatrix} \tag{3.1.4}$$

when the simulation uses a forecast interval of h_{FW} hours these matrices become:

$$\boldsymbol{C_{pp}} = \begin{bmatrix} \boldsymbol{C_{pp,h}} & & \\ & \boldsymbol{C_{pp,h}} & \\ & & \ddots \end{bmatrix} \qquad \boldsymbol{d_{pp}} = \begin{pmatrix} \boldsymbol{d_{pp,h}} \\ \vdots \\ \boldsymbol{d_{pp,h+h_{FW}}} \end{pmatrix} \tag{3.1.5}$$

Finally, as done with the $\boldsymbol{K_D}$ coefficient, the lines have to be normalized to prevent the connections with greater transmission capacity have a higher weight on the norm of the residual to be minimized. Therefore $\boldsymbol{C_{pp}}$ and $\boldsymbol{d_{pp}}$ are multiplied by $\boldsymbol{K_L}$:

$$\boldsymbol{K_L}(i) = \frac{\sum_{l=i}^{N_l} \boldsymbol{T_C}(i)}{\boldsymbol{T_C}(i)} \tag{3.1.6}$$

To summarize, for each section of the code, x_{pp} is a approach that does not impact on the demand coverage obtained with the "original" version of COMESE (x_1), but transmission lines and generators are exploited such as to limit the power exchanges among the zones.

Changing the C matrix

In this case, differently from before, a post-processing section is not included, but the $\boldsymbol{C}$ matrix and the $\boldsymbol{d}$ vector are modified directly: in particular, new rows are added so that the objective function includes the minimisation of both the residual demand and the power flow among zones. So, considering a single hour h, the new form ($\boldsymbol{C'_h}$ and $\boldsymbol{d'_h}$) of $\boldsymbol{C_h}$ and $\boldsymbol{d_h}$ is:

$$\boldsymbol{C'_h} = \begin{bmatrix} \boldsymbol{C_h} \\ \boldsymbol{C_{minPF,h}} \end{bmatrix} \qquad \boldsymbol{d'_h} = \begin{pmatrix} \boldsymbol{d_h} \\ \boldsymbol{d_{minPF,h}} \end{pmatrix} \tag{3.1.7}$$

where $\boldsymbol{C_h}$ and $\boldsymbol{d_h}$ are the "original" parts described in section 2.2.2, whereas $\boldsymbol{C_{minPF,h}}$ and $\boldsymbol{d_{minPF,h}}$ are defined as follow:

$$\boldsymbol{C_{minPF,h}} = \begin{bmatrix} \boldsymbol{I}_{N_I \times N_I} & \boldsymbol{0}_{N_I \times N_Z} \end{bmatrix} \qquad \boldsymbol{d_{minPF,h}} = \begin{pmatrix} -\boldsymbol{PF}_{former}(h,1) \\ \vdots \\ -\boldsymbol{PF}_{former}(h,N_I) \end{pmatrix} \tag{3.1.8}$$

Basically, up to this point, it is like adding $\boldsymbol{C_{pp,h}}$ and $\boldsymbol{d_{pp,h}}$ respectively to $\boldsymbol{C_h}$ and $\boldsymbol{d_h}$. $\boldsymbol{C_h}$ and $\boldsymbol{d_h}$ are multiplied by $\boldsymbol{K_{D_h}}$ (see eq. 2.2.7), $\boldsymbol{C_{minPF,h}}$ and $\boldsymbol{d_{minPF,h}}$ by $\boldsymbol{K_L}$ (see eq. 3.1.6), but, in order to give priority to residual demand minimization, $\boldsymbol{C_{minPF,h}}$ and $\boldsymbol{d_{minPF,h}}$ have to be weighted with a suitable coefficient ($K'_{L,h}$), otherwise, when *lsqlin* minimises the norm of the residual priority would be given to the power flow reduction instead of covering the demand. Several options were taken into consideration to find

the optimal value of $K'_{L,h}$.

- the simplest solution is choosing a constant term that must be small enough so that the minimization of power flows is a secondary objective with respect to balancing supply and demand, but not too small otherwise the solver ignores $\boldsymbol{C_{h,2}}$ and $\boldsymbol{d_{h,2}}$ (or it would be necessary to increase its precision excessively). As shown later $K'_L = 10^{-3}$ seems to be a good value, but it is an empiric coefficient that might not be suitable for every situation. For instance, in the mid-analysis section, $\boldsymbol{d_h}$ can frequently be small (and have some elements equal to zero) and so the solver finds an optimum compromise between minimizing the residual associated with $\boldsymbol{d_h}$ and that associated with $\boldsymbol{d_{minPF,h}}$.

- another option is choosing a term that varies according to $\boldsymbol{d_h}$ which, in most of the code sections, represents the residual demand or deficit:

$$K'_{L,h} = 10^{-3} \frac{\sum_{z=1}^{N_Z} \boldsymbol{d_h}(z)}{\sum_{i=1}^{N_I} \boldsymbol{T_C}(i)} \tag{3.1.9}$$

  in this way the minimization of the power flows should always be subordinated to demand balancing. However $\boldsymbol{d_h}(z)$ could be very different among the various zones, so it could happen that $\sum_{z=1}^{N_Z} \boldsymbol{d_h}(z)$ is relatively big, although with a small value of $\boldsymbol{d_h}(z)$, therefore for that zone the prioritising the power flow minimisation to residual demand would not be possible.

- alternatively K_L con be set to:

$$K'_{L,h} = 10^{-3} \frac{\min\{\boldsymbol{d_h} \neq 0\}}{\sum_{i=1}^{N_I} \boldsymbol{T_C}(i)} \tag{3.1.10}$$

  by choosing the minimum between the non-zero values of $\boldsymbol{d_h}$ the problem of the former approach is avoided. On the other hand, it could happen that the numerator become very small, therefore some terms in system (2.2.3) could have a very different order of magnitude with respect to the others (again this is more likely when $\boldsymbol{d_h}(z)$ is not similar between the various zones). This fact can lead to weight $\boldsymbol{C_{h,2}}$ and $\boldsymbol{d_{h,2}}$ with a too small term, but even to some convergence issues as explained in appendix A.1.

To summarize all the alternatives have their pros and cons, but they actually lead to very similar results. Anyway the second one is the one that seems to work better in most of the cases. The comparison of the two approaches for power flows minimization presented in the next paragraph was made implementing this option.

Comparison of the two approaches for power flows minimization

To compare the two approaches, the results obtained with three different scenarios are now presented. However, during the thesis work, several tests were carried out that led to conclusions consistent with those reported here. From now on, the name of the scenarios is defined by the letter *S* followed by acronyms which identifies the peculiarities of each scenario. For instance *RES* means that only renewable energy sources contribute to the power mix, whereas *Fus/RES* scenarios also consider the presence of fusion power plants. As regards the installed power of the generation technologies in the zones, *S-Fus/RES* will be described in detail in chapter 4, whereas *S-Fus/RES-3D* has the same input data, but the demand curve is scaled by a factor 3 to obtain a scenario where meeting the load is very difficult or even impossible in certain hours. In this way the interconnections among the zones result particularly stressed by playing a crucial role for the coverage of the demand. *S-Fus/RES* and *S-Fus/RES-3D* are based on the model of the Italian transmission grid representation currently used in the management of the electricity market (see the left picture of figure 2.3). The value of the capacity of the transmission lines are taken from [23] and summarized in table 3.1 Instead only zones North, Centre-North and Centre-South are analyzed in

Interconnection	transmission capacity [GW]
N-CN	3,9
CN-CS	2,5
CN-Sar	1
CS-S	4,6
CS-Sar	0,9
S-Sic	1,2

Table 3.1: Transmission capacity values. Current grid model

S-3Z-Fus/RES, and the capacity of the two lines connecting these zones is increased significantly (table 3.2) in order to highlight the effect of power flows minimization. The three zones in *S-3Z-Fus/RES* are identical to the corresponding ones in *S-Fus/RES*.

Interconnection	transmission capacity [GW]
N-CN	10
CN-CS	9

Table 3.2: Transmission capacity values. 3 zones model

The LCOTE (which depends on the total energy produced by the various technologies), the energy produced by biogas-fired dispatchable generators (E_{biogas}) and the final residual demand ($E_{unserved}$) are the quantities used to check that the minimization of power flows does not affect the overall results but only how the grid is exploited. The comparison of the two alternatives also takes into account the computational time, which obviously depends on the computer used (all the simulations were run on a i7-11th generation 16 GB RAM machine), so it is presented only as an indicative parameter to compare different solutions. Three different code version are tested:

- original: the original code version as presented in chapter 2.
- minPF,pp: the power flows minimization is implemented using the post-processing approach.
- minPF,newC: the power flow minimization is implemented changing $\boldsymbol{C}$ and $\boldsymbol{d}$.

Figure 3.1 shows the duration curves of the power flows on the lines in *S-3Z-Fus/RES*. In this case is apparent how it is possible to highly reduce the power exchanges between the zone without influencing the electricity cost (see table 3.3). Indeed the new modifications affect only how the generated power is distributed among the zones, but not the overall amount of energy produced by the various technologies. minPF,pp and minPF,newC lead to very similar results, as can be seen from the form of the duration curves and the total energy transmitted on the lines E_{line}, summarized in table 3.4.

	original	minPF,pp	minPF,newC
time [s]	300	480	440
LCOTE [c€/kWh]	10,14	10,14	10,14
E_{biogas} [TWh]	33, 48	33, 52	33, 51
$E_{unserved}$ [TWh]	0	0	0

Table 3.3: *S-3Z-Fus/RES*, overall results

Similar conclusion can be drawn from the analysis of *S-Fus/RES*: the duration curve of figure 3.2, and table 3.6 clearly show how both minPF,pp and minPF,newC are effective

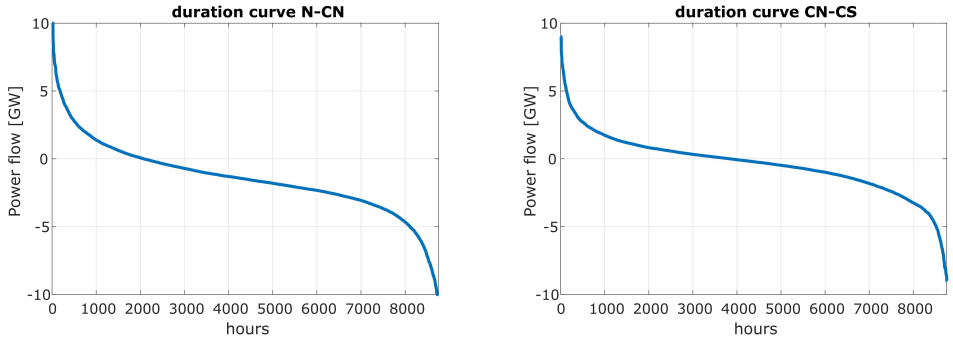

(a) Duration curves. Original version

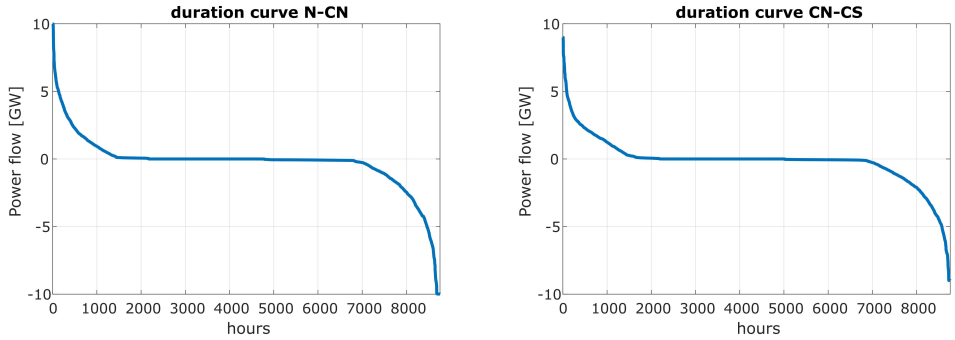

(b) Duration curves. minPF,pp

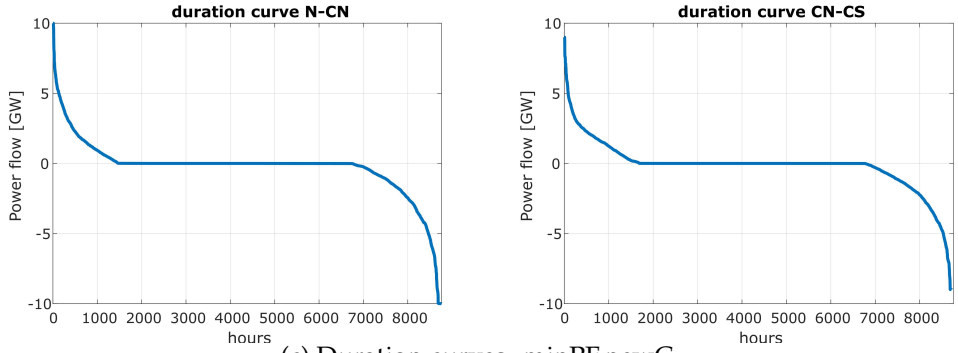

(c) Duration curves. minPF,newC

Figure 3.1: *S-3Z-Fus/RES* with and without power flows minimization

in reducing the transmitted power on the grid. Actually minPF,pp is a more precise and general approach and it was used as benchmark to test different values of $K'_{L,h}$: minPF,newC leads to slightly higher power flows, meaning that, for some hours during the year, the weight given to $\boldsymbol{C_{minPF}}$ and $\boldsymbol{d_{minPF}}$ is too little with respect to the solver precision. Nevertheless it was chosen to keep the expression of equation (3.1.9) so that it is ensured that demand balancing has the priority. Indeed if $K'_{L,h}$ is increased *lsqlin* could prioritize minimizing the load on the line rather than the residual deficit. As regards the LCOTE (table 3.5), a little increase can be observed when adopting the power flows minimization: this is due to a growth in the energy produced by turbo-gas generators. The reasons behind this behavior lie in the fact that the way of performing

	E_{line} [TWh]		
Interconnection	Original	minPF,pp	minPF,newC
N-CN	20,52	8,198	8,192
CN-CS	13,61	8,020	7,914

Table 3.4: *S-3Z-Fus/RES*, total energy transmitted on the lines

storage discharge may affect the charge of the same technology in the following hours, as better explained in chapter 3.2.2. Indeed if, for instance, minPF,pp is removed from the storage section the resulting LCOTE and E_{biogas} are exactly identical to the ones of the original version.

	original	minPF,pp	minPF,newC
time [s]	1100	1860	1530
LCOTE [c€/kWh]	12,18	12,23	12,22
E_{biogas} [TWh]	24,16	24,32	23,41
$E_{unserved}$ [TWh]	0	0	0

Table 3.5: *S-Fus/RES*, overall results

	E_{line} [TWh]		
Interconnection	Original	minPF,pp	minPF,newC
N-CN	15,33	8,91	1,052
CN-CS	10,42	7,42	7,91
CN-Sar	5,07	3,27	3,57
CS-S	20,26	14,94	15,17
CS-Sar	3,35	2,04	2,12
S-Sic	4,12	2,75	2,73

Table 3.6: *S-Fus/RES*, total energy transmitted on the lines

In *S-Fus/RES-3D*, as expected, the effect of power flows reduction, although still present, is not as evident as in the previous cases (figure 3.3). In fact, since it is very difficult to balance the demand, in most of the cases the power exchanges among the zones are not "unmotivated", but required to reduce the residual load. As further confirmation, it can be seen that the hours of congestion (i.e., when the power on the line I reaches $\boldsymbol{T_C}(I)$) are very similar in the various alternatives. Table 3.7 shows how the consideration regarding the LCOTE described above apply also in this case.

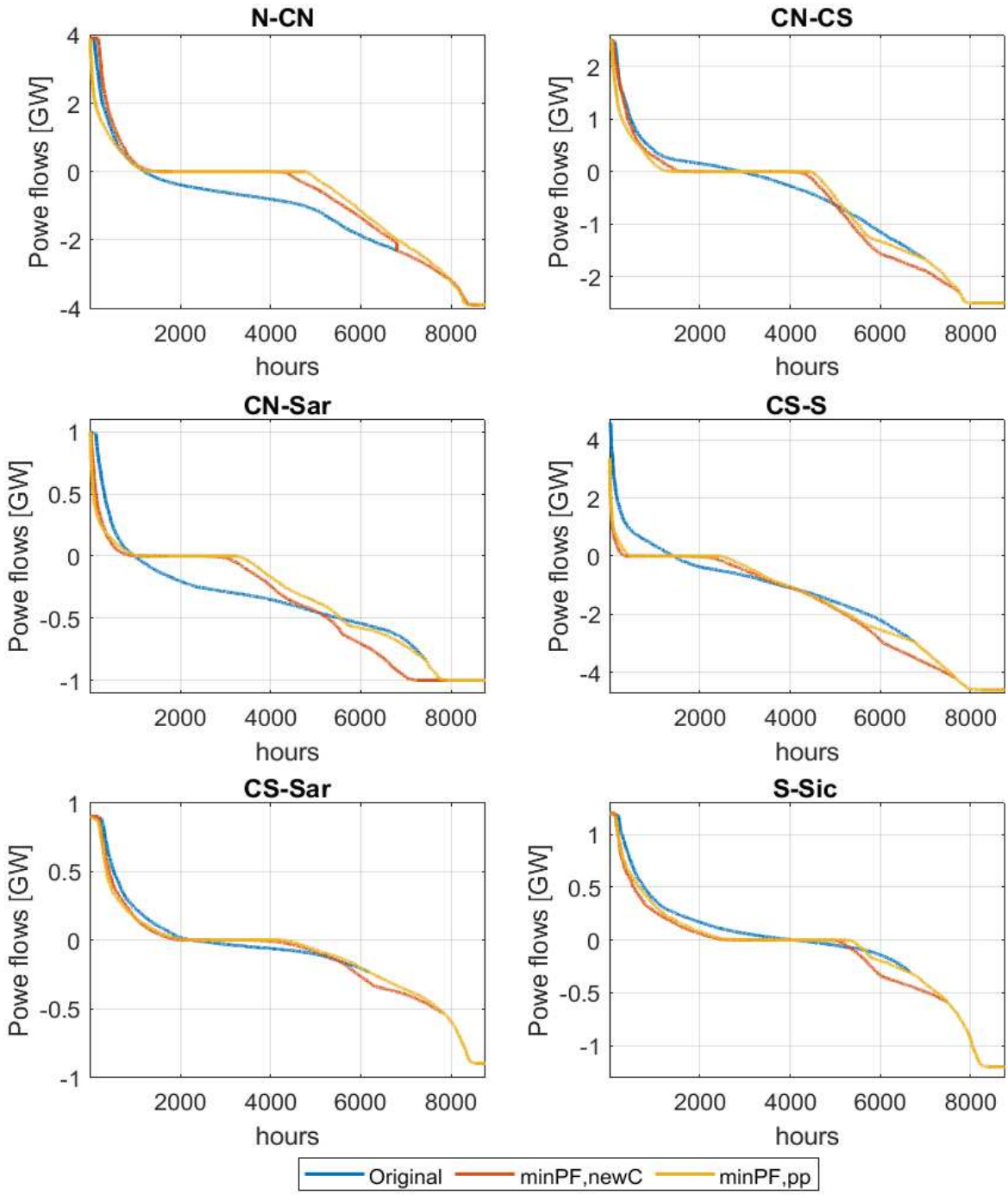

Figure 3.2: *S-Fus/RES* with and without power flows minimization

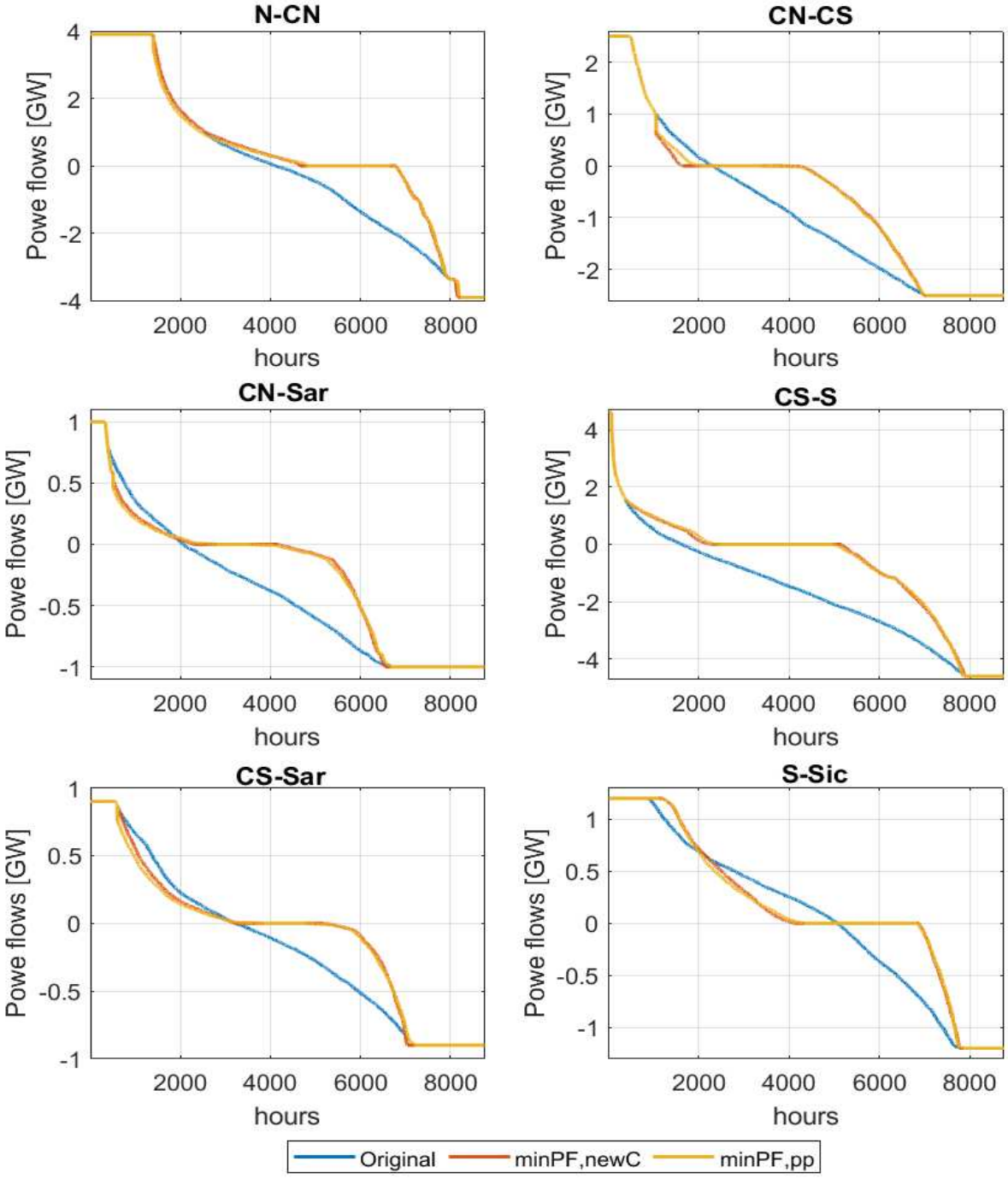

Figure 3.3: *S-Fus/RES-3D* with and without power flows minimization

	original	minPF,pp	minPF,newC
time [s]	1210	1950	1590
LCOTE [c€/kWh]	15,45	15,48	15,48
E_{biogas} [TWh]	889, 4	890, 1	890, 1
$E_{unserved}$ [TWh]	150, 6	151, 5	151, 5

Table 3.7: *S-Fus/RES-3D*,overall results

	E_{line} [TWh]		
Interconnection	Original	minPF,pp	minPF,newC
N-CN	17, 46	16, 03	16, 13
CN-CS	13, 67	9, 55	9, 40
CN-Sar	5, 54	4, 02	3, 99
CS-S	19, 55	11, 23	11, 11
CS-Sar	4, 23	3, 54	3, 54
S-Sic	6, 12	4, 46	4, 50

Table 3.8: *S-Fus/RES-3D*, total energy transmitted on the lines

To summarize both minPF,pp and minPF,newC are valid approaches to minimize power flows or, in any case, to establish a precise logic for the grid management. minPF,newC turns out to have a lower computational burden because it does not involve adding a post-processing section. Despite this, minPF,pp is preferred when a more accurate analysis needs to be performed: although it leads to an increase of about 60-70 percent in the running time, it is applicable to any case, without the need to calibrate the value of coefficients such as K'_L .

3.1.2 Grid losses

Introducing joule losses in the grid model is not so simple because, in general, this leads to a non-linear problem (whereas all the code is written with liner equations and constraints). In order to get a detailed description, while keeping the system linear, a piecewise linear approximation could be used, adopting a discrete set of (constant) line efficiencies, each associated with a defined load range on the line [32]. Here is examined the simplest case, where a constant line efficiency η_L (different from 1) is used regardless of the amount of power flowing on the line. Even in this case , there is the need to know the direction of the power flow so that the line losses can be allocated to the actual receiving node: the solution adopted requires splitting of each transmission line into

two: one can carry only positive flows, whereas the other only negative.

Consider the example of figure 3.4 of a system with just three zones and two transmission lines. When line efficiency is considered the incidence matrix of "forward lines" M_{T_p} is different from the one of "backwards lines" M_{T_n}. For each "forward line" M_{T_p} has -1 in the position corresponding to the starting node and η_L in the position corresponding to the receiving node. In M_{T_n}, which is related to interconnections that can carry only "negative" power flows, there is the need to switch the role of starting and receiving nodes:

$$\boldsymbol{M_T} = \begin{bmatrix} \boldsymbol{M_{T_p}} & \boldsymbol{M_{T_n}} \end{bmatrix} = \begin{bmatrix} -1 & 0 & -\eta_L & 0 \\ \eta_L & -1 & 1 & -\eta_L \\ 0 & \eta_L & 0 & 1 \end{bmatrix} \tag{3.1.11}$$

Therefore it's clear that the variables associated with the power flows double and

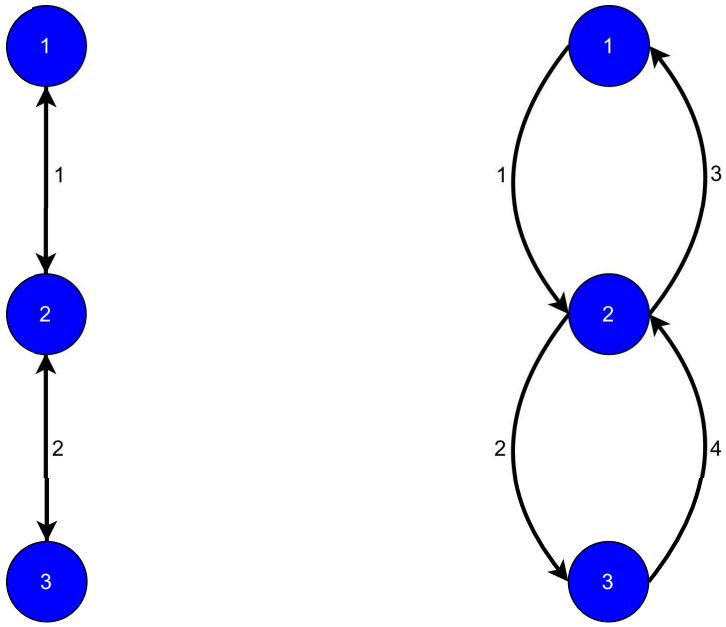

Figure 3.4: The left figure shows a system where line losses are neglected: each line can carry power in both directions. With a constant η_L the number of lines double and each one allows power flows only in one direction

the related upper ($u_{b,lines}$) and lower ($l_{b,lines}$) bounds are updated consequentially.

Keeping the same example as above and considering only hour h one gets:

$$l_{b,lines_h} = \begin{bmatrix} 0 - \boldsymbol{PF}_{former}(h,1) \\ 0 - \boldsymbol{PF}_{former}(h,2) \\ -\boldsymbol{T_C}(3) - \boldsymbol{PF}_{former}(h,3) \\ -\boldsymbol{T_C}(4) - \boldsymbol{PF}_{former}(h,4) \end{bmatrix} \quad u_{b,lines_h} = \begin{bmatrix} \boldsymbol{T_C}(1) - \boldsymbol{PF}_{former}(h,1) \\ \boldsymbol{T_C}(2) - \boldsymbol{PF}_{former}(h,2) \\ 0 - \boldsymbol{PF}_{former}(h,3) \\ 0 - \boldsymbol{PF}_{former}(h,4) \end{bmatrix} \tag{3.1.12}$$

So, it is not completely true that the first two positive lines can carry only positive flows, and the other two only negatives, because each limit is updated with the respective value in $\boldsymbol{PF}_{former}$. In this way the solver has the possibility to recover previous losses if the flow needs to be reversed with respect to the one obtained in the former section. The net power flows are computed only at the end of the main for-cycle by summing the values of the forward and backwards flows. It should be noted that, when introducing grid losses, is mandatory to minimize the random power flows as explained in 3.1.1 (otherwise there would be unmotivated lost energy along the grid) and also the storage charge section needs to be modified (storage is treated in the following section 3.2).
Anyway, because of the doubling of the variables associated with the transmission lines, the computational burden significantly increases when modelling (in a simplified way) grid losses. Table 3.9 summarizes the result obtained with *S-3Z-Fus/RES* and *S-Fus/RES* when transmission losses amount to 5% of the total transmitted energy. Δ_{LCOTE} is the percentage variation on the LCOTE with respect to the case without transmission losses. The power flows minimization approach used is minPF,pp, so the duration curves of the line loads are almost identical to the one shown in figure 3.1 and 3.2. The original storage charge formulation is replaced with New charge1 (see paragraph 3.2.1). The running time nearly double with respect to the original case, and the impact on the LCOTE is limited. Introducing a linear piecewise approximation would lead to

	S-3Z-Fus/RES	*S-Fus/RES*
time [s]	550	2120
LCOTE [c€/kWh]	10,20	12,30
Δ_{LCOTE} [%]	0,7	1

Table 3.9: Running time and electricity cost when 95% line efficiency is considered

a worsening of this issue: for instance, using two different efficiencies, one when the $\boldsymbol{PF}$ is between 0-50% of $\boldsymbol{T_C}$ and the other when $\boldsymbol{PF}$ is greater than 50% of $\boldsymbol{T_C}$, implies to double (again) the lines and the related variables.

3.2 Storage Management

3.2.1 Storage Charge

As explained in paragraph 2.2.2, in the "original" version of COMESE storage charge is performed by minimizing the energy surplus resulting from the *BMR* section and managing storage plants like loads in the various zones. This approach has some drawbacks:

- It cannot be used when grid losses are taken into account, because the solver, in order to minimize the total surplus, might prioritise the power flows increase - because of the losses -to storage charging.
- It is incompatible with both the flow minimization methods explained in section 3.1.1. Indeed they aim to preserve the residual $\boldsymbol{R}$ obtained with the "original" version, but, in the case of storage charge, the residual surplus ($\boldsymbol{P_{OG}}$) is already affected by an useless power grid utilization.
- There isn't the possibility to control how the excess energy is distributed among zones: for instance it could be useful to prioritize the charging of some zones with respect to others.

To address these issues, a new charging methodology has been implemented whereby system (2.2.3) is defined to minimize the residual capacity still available in the storage plants, by using the surplus energy coming from the *BMR* section. Two alternatives are presented where the latter is a simplified version of the former but allows an important reduction on the computational burden.

"New charge1"

In order to introduce this new storage charge formulation it is useful to remind how $\boldsymbol{A}$ and $\boldsymbol{b}$ are built in the "original" storage section of COMESE. The number of rows (m) of $\boldsymbol{A}$ and $\boldsymbol{b}$ is equal to the total number of charge intervals (N_{ch}), within the forecast interval and considering each zone, times the number of storage technologies N_s. Considering a generic row of the system $\boldsymbol{A} \cdot \boldsymbol{x} \leq \boldsymbol{b}$, which involves the *s-th* storage technology, in zone z, with charge efficiency $\eta_{ch,s}$ and a charge interval (i.e. a sequence of surplus hours) from hour h to hour $h_{ch} + h$, the constraint states that the cumulative charging (or input) power $\boldsymbol{Pch_s}$ cannot exceed the capacity of the storage system $\boldsymbol{Cap_s}$:

$$\sum_{i=h}^{h_{ch}+h} \boldsymbol{Pch_s}(i,z) \cdot \eta_{ch,s} \leq \boldsymbol{Cap_s}(z) \tag{3.2.1}$$

Consequently the term $\boldsymbol{A \cdot x - b}$ represents precisely the residual capacity of each storage plant available at the end of each charge interval, and so the objective function of this new charge approach (i.e. $\boldsymbol{C_{ch1}}$ and $\boldsymbol{d_{ch1}}$) can be built starting from $\boldsymbol{A}$ and $\boldsymbol{b}$ of the "original" version. The only difference is that different storage plants, within the same zone and charge interval, are "aggregated" in the same row of $\boldsymbol{C_{ch1}}$ and $\boldsymbol{dch1}$, summing their contribution to the total stored energy and storage capacity of that zone; in this way the solver automatically gives priority to charging the technology with the best $\eta_{ch,s}$:

$$\boldsymbol{C_{ch1}}(i,j) = \sum_{k=(i-1)N_s+1}^{i \cdot N_s} \boldsymbol{A}(k,j), \quad \boldsymbol{d_{ch1}}(i) = \sum_{k=(i-1)N_s+1}^{i \cdot N_s} \boldsymbol{b}(k), \quad \text{with } i = 1, 2, \ldots, N_{ch} \tag{3.2.2}$$

Then, as done with K_D and K_L, a K_S coefficient must be to be introduced so that each zone has the same weight independently of the total maximum storage capacity in the zone (otherwise, when minimising the residual in the least squares sense, the solver would always prefer to charge the largest storage plants):

$$\boldsymbol{K_S}(z) = \frac{\sum_{z=1}^{N_Z} \sum_{s=1}^{N_s} \boldsymbol{Cap_s}(z)}{\sum_{s=1}^{N_s} \boldsymbol{Cap_s}(z)} \tag{3.2.3}$$

As mentioned above, with this formulation it is possible to prioritize the charging of some zones: if the i charge interval is considered, which involves zone z and ends at hour h_{end}, $\boldsymbol{C_{ch1}}(i)$ and $\boldsymbol{d_{ch1}}(i)$ are multiplied by an additional coefficient $\boldsymbol{K_{ch}}(i)$ defined as:

$$\boldsymbol{K_{ch}}(i) = \frac{\sum_{h=h_{end}+1}^{h_f} \boldsymbol{Def}(h,z)}{\sum_{h=h_{end}+1}^{h_f} \boldsymbol{D}(h,z)} + 0.1 \max\{\boldsymbol{K_{ch}}\} \tag{3.2.4}$$

where h_{end} is the last hour of the forecast interval. The term $0.1 \max\{\boldsymbol{K_{ch}}\}$ is needed to prevent $\boldsymbol{K_{ch}}$ from being zero (0.1 appears to be a good choice after some tests). In this way, the zones with a higher deficit (compared to the demand) in the hours following the

charge interval have charging priority. Consequently the interconnections between the zones are better exploited because during surplus hours the energy is shifted where it will be needed the most, so that during deficit hours there is more transmission capacity available for the management of dispatchable generators. As regards the linear bounds and constraints they are identical to the ones of the "original" version; they only differ on the input storage power, hour by hour, that cannot exceed the available surplus power: this is simply done by using $\boldsymbol{C}$ and $\boldsymbol{d}$ defined in the original version of storage charge:

$$\boldsymbol{A_{ch1}} = \begin{bmatrix} \boldsymbol{A} \\ \boldsymbol{-C} \end{bmatrix} \quad \boldsymbol{b_{ch1}} = \begin{pmatrix} \boldsymbol{b} \\ \boldsymbol{-d} \end{pmatrix} \tag{3.2.5}$$

As shown later this solution leads to positive results in terms of LCOTE and dispatchable energy reduction mainly in scenarios where the demand balancing is very hard and with an important amount of storage capacity available.

"New charge2"

This storage charge formulation follows the same approach of the former, but all the storage plants and charge intervals are "joint" together, so that the objective is now the minimization of the overall residual storage capacity Cap_{res}:

$$Cap_{res} = \sum_{i=1}^{N_{ch}} \sum_{z_i} \sum_{s=1}^{N_s} \left(\boldsymbol{Cap_s}(z) - \sum_{h_i} \boldsymbol{Pch_s}(h,z) \cdot \eta_{ch,s} \right) \tag{3.2.6}$$

where z_i and h_i are the zones and hours involved in the $i-th$ charge interval, respectively. Minimizing equation (3.2.6) is equivalent to the maximization of the cumulative storage input power, with the usual constraint that the energy stored cannot exceed the capacity of the plant. Therefore the objective function is linear and *linprog* can be used: following the same notation as in appendix A.2, $\boldsymbol{f}$ can be computed easily by summing column-wise all the rows of $\boldsymbol{A}$ or $\boldsymbol{C_{ch1}}$ with changed sign:

$$\boldsymbol{f}(j) = -\sum_{i=1}^{m} \boldsymbol{A}(i,j) = -\sum_{i=1}^{N_{ch}} \boldsymbol{C_{ch,1}}(i,j) \tag{3.2.7}$$

Moreover all the bounds and constraints are identical to the ones of "New charge1", so it's possible to implement both solutions and let the user decide which to use. Obviously in this case there is not the possibility to prioritize the charge of some zones

with respect to others, but a great advantage is the lower computational time.
Finally it should be noted that both "New charge1" and "New charge2" are compatible with the modelin of line losses, and the power flows minimization methods presented in 3.1.1 can be easily integrated. For instance, if $\boldsymbol{C_{minPF}}$ is employed, $\boldsymbol{C_{ch1}}$ becomes

$$\boldsymbol{C'_{ch1}} = \begin{bmatrix} \boldsymbol{C_{ch1}} \\ \boldsymbol{C_{minPF}} \end{bmatrix} \tag{3.2.8}$$

whereas *lsqlin* must be used also in "New charge2" obtaining

$$\boldsymbol{C'_{ch2}} = \begin{bmatrix} f \\ \boldsymbol{C_{minPF}} \end{bmatrix} \tag{3.2.9}$$

Results

In this section the results obtained with the upgrades on storage charge management are shown. The same scenarios used in section 3.1.1 are tested also in this case.

		Original	New charge1	New charge2
S-3Z-Fus/RES	time [s]	300	320	250
	LCOTE [c€/kWh]	10,14	10,14	10,14
	E_{biogas} [TWh]	33, 48	33, 46	33, 51
	$E_{unserved}$ [TWh]	0	0	0
S-Fus/RES	time [s]	1100	1180	910
	LCOTE [c€/kWh]	12,18	12,15	12,18
	E_{biogas} [TWh]	24, 16	24, 08	24, 12
	$E_{unserved}$ [TWh]	0	0	0
S-Fus/RES-3D	time [s]	1210	1300	1020
	LCOTE [c€/kWh]	15,45	15,32	15,45
	E_{biogas} [TWh]	889, 4	887, 1	889, 1
	$E_{unserved}$ [TWh]	150, 6	144, 9	150, 4

Table 3.10: New storage charge: results

Table 3.10 summarizes the most relevant results. New charge2, i.e. using *linprog* instead of *lsqlin* to perform storage charge, is very effective at speeding up the code, indeed a reduction of about 15% in the running time can be observed in every scenarios, and the

other quantities do not change with respect to the original case. New charge1 does not have a great impact on the analysis of *S-3Z-Fus/RES* and *S-Fus/RES*, because in these cases the demand is already easily balanced using the original version of COMESE. On the other hand, in *S-Fus/RES-3D* both the LCOTE and the total unserved load decrease when adopting a "smarter" charge, in particular it is possible to recover more than 3% of $E_{unserved}$. This is due to a better allocation between the zones of the surplus energy resulting from the *BMR* exploitation, which leads either to reduce the turbo-gas generators power output when the demand is met, or, with equal biogas generation, to lower the residual deficit. Thus, the effectiveness of this modification depends on the scenario under analysis: it is particularly suitable when, together with the presence of a large share of non-programmable generators, storage is crucial to meet the demand, and constraints on transmission capacity strongly influence the behavior of the system.

3.2.2 Storage Discharge

The way of performing discharge of storage plants could influence the possibility of charging the same technologies in the following surplus hours. For example, let's consider the system in the left side of figure 3.4 and assumes that a technique of power flows minimization has been adopted: when the deficit is concentrated in zone*1* the storage will discharge mainly in zone*1*, whereas there might be the possibility of generating power in zone*3* and moving it "upwards". But, if in the following hours the surplus is concentrated in zone*3*, there is little residual storage capacity available in zone*3*, and the transmission capacity of line*2* could be insufficient to carry the energy towards zone*1*; therefore the total charged energy is potentially less than the one obtained if, during the discharge operation, the storage plants in zone*3* had been used to cover the load (or a portion of it) of zone*1*. An idea to try to solve this problem could be to give discharge priority to the zones that will have the most energy surplus. Mathematically, as done for the minimization of power flows, this is implemented by adding new rows to $\boldsymbol{C}$ and $\boldsymbol{d}$:

$$\boldsymbol{C}_{new} = \begin{bmatrix} \boldsymbol{C} \\ \boldsymbol{C}_{dch1} \end{bmatrix} \quad \boldsymbol{d}_{new} \begin{bmatrix} \boldsymbol{d} \\ \boldsymbol{d}_{dch1} \end{bmatrix} \tag{3.2.10}$$

The number of rows of $\boldsymbol{C}_{dch1}$ is equal to the total number of discharge interval N_{dch}, within the forecast interval and considering each zone (a discharge interval is a continuous sequence of deficit hours). The term $\boldsymbol{C}_{dch1} \cdot \boldsymbol{x}$ represents the output energy

during each discharge interval considering also the round-trip efficiency $\eta_{ch,s} \cdot \eta_{dch,s}$ of the storage technologies involved:

$$\boldsymbol{C_{dch1,i}} \cdot \boldsymbol{x} = \sum_{h_i} \sum_{s=1}^{N_s} \left(\boldsymbol{Pdch_s}(h, z_i) \cdot \eta_{ch,s} \cdot \eta_{dch,s} \right) \quad with\, i = 1, \ldots, N_{dch} \tag{3.2.11}$$

where $\boldsymbol{C_{dch1,i}}$ is the i_{th} row of $\boldsymbol{C_{dch1}}$, h_i are the hours within the $i_t h$ discharge interval, z_i is the zone involved in the $i_t h$ discharge interval. Instead the $i-th$ raw of $\boldsymbol{d_{dch1}}$ is computed as the sum of the surplus power following the discharge interval (which ends at hour $h_{end\,dch_i}$):

$$\boldsymbol{d_{dch1}}(i) = \sum_{h=h_{end\,dch_i}}^{h_f} \boldsymbol{Surp}(h, z_i) \tag{3.2.12}$$

In this way the solver tries to discharge the storage so that the output energy in a given zone is as similar as possible to the future energy surplus in that zone, and, within each zone, priority is given to the technology that has the best round-trip efficiency. But, as done with $\boldsymbol{C_{minPF,h}}$ (see section 3.1.1), also in this case there is the need to weight $\boldsymbol{C_{dch1}}$ and $\boldsymbol{d_{dch1}}$ so that they do not influence the proper demand coverage. For this purpose the $\boldsymbol{K_{dch}}$ is introduced as follow:

$$\boldsymbol{K_{dch}}(i) = 10^{-3} \cdot \frac{\min\left\{Def_1 \neq 0\right\}}{\sum\limits_{k=1+N_s(i-1)}^{2i} \boldsymbol{b}(k)} \tag{3.2.13}$$

where $\boldsymbol{b}$ is exactly the right hand side of the inequality constraints $\boldsymbol{A} \cdot \boldsymbol{x} \leq \boldsymbol{b}$ (that are equal to the one of the original storage discharge section): $\boldsymbol{b}(k)$ is the total energy stored in a single storage technology of one zone in the hours preceding the *k-th* discharge interval. This approach leads to a slight reduction in the dispatchable energy output due to an increase of the energy stored during surplus hours; on the other hand it is not compatible with power flows minimization because, during the storage discharge section, the grid is used following the logic explained just above.

Results

In this section the results obtained with the upgrades on storage discharge management are shown. The same scenarios used in 3.1.1 are tested also in this case. Finally it is shown how the combined use of "New charge1" and new storage discharge (called "new storage") impacts on the final results of the scenarios under analysis. From table

		Original	New discharge	New storage
S-3Z-Fus/RES	time [s]	300	350	370
	LCOTE [c€/kWh]	10,14	10,14	10,14
	E_{biogas} [TWh]	33,48	33,48	33,41
	$E_{unserved}$ [TWh]	0	0	0
S-Fus/RES	time [s]	1100	1290	1400
	LCOTE [c€/kWh]	12,18	12,17	12,14
	E_{biogas} [TWh]	24,16	24,10	23,94
	$E_{unserved}$ [TWh]	0	0	0
S-Fus/RES-3D	time [s]	1210	1360	1480
	LCOTE [c€/kWh]	15,45	15,43	15,32
	E_{biogas} [TWh]	889,4	888,6	887,0
	$E_{unserved}$ [TWh]	150,6	149,6	144,6

Table 3.11: New storage discharge: results

3.11, it can be seen that this new storage discharge approach does not lead to substantial changes in the final results (the lowering in the LCOTE is negligible). This is particularly true for *S-3Z-Fus/RES*: in this case, the line capacities are relatively high and the demand can be easily covered, therefore the simulation is nearly unaffected by the constraints due to the introduction of the grid; therefore it is not important how the energy stored and supplied by the storage plants is distributed between the zones. As the transmission grid constraints have a larger impact on system behavior, the changes on storage operation also become more relevant, and a slight improvement of the LCOTE and $E_{unserved}$ can be observed. Anyway, it should be noted that all the scenarios presented are characterized by a high share of renewable energy plants and installed storage capacity (for instance *S-Fus/RES* assumes the presence of 1400 GWh of electrochemical storage capacity for a total of 175 GW of installed power). Therefore, for many hours during the year, there is a high energy surplus resulting from the *BMR* exploitation and storage plants play a crucial role in the management of dispatchable generators and in demand balancing, especially when it is difficult to meet the load. If scenarios with less available photovoltaic and storage power are studied the modifications on storage operation are less impactful on the final results.

3.3 New formulation of dispatch optimization

If the code is used to perform not only a simulation but also an optimization of the system (see 2.4), the running time could be of several hours, even days: in this case, it is important to reduce as much as possible the computation cost, without affecting in a relevant way the final outputs that are involved in the optimization algorithm (for instance LCOTE, hours of unserved load, and total energy produced by biogas fired dispatchable generators). The results from the former section show that increasing the level of detail in the storage management, through a smarter charge and discharge operation, doesn't lead to big changes in the LCOTE (although a slight improvement in the energy cost is always observed), while employing *linprog* has a significant impact on the computational time. At the same time introducing power flows minimization (as explained in 3.1.1) does not influence significantly the overall final results, but it is useful to analyze how the system would behave under a specific logic of grid management, at the cost of reducing code speed.

One of the main factors impacting the computational complexity of the code is the fact that, in each section, a constrained linear least-squares system must be solved, which results into a quadratic programming problem (see Appendix A.1). In order to move to linear programming, an approach similar to the one used with "New charge2" can be used. Instead of minimizing the norm of the vector whose components are the residual demand of each zone and hour, the idea is to maximize the overall energy output by gathering together all zones and hours within the forecast interval, with the additional constraint that the generated power cannot exceed the deficit to be covered in the each zone and hour. Mathematically, considering a generic section *sec* different from storage, the aim is to maximize the sum of the generated power P_{sec}

$$\sum_{z=1}^{N_Z} \sum_{i=h}^{h+h_{FW}} \boldsymbol{P_{sec}}(i,z) \tag{3.3.1}$$

therefore, using *linprog*, this can be simply achieved by allowing

$$\boldsymbol{f_{sec}}(j) = -\sum_{k=1}^{m} \boldsymbol{C_{sec}}(k,j) \tag{3.3.2}$$

where m is the number of rows of $\boldsymbol{C_{sec}}$. Finally $\boldsymbol{C_{sec}}$ and $\boldsymbol{d_{sec}}$ are added to the inequality

constraints:

$$A'_{sec} = \begin{bmatrix} A'_{sec} \\ C_{sec} \end{bmatrix} \quad b'_{sec} = \begin{pmatrix} b_{sec} \\ d_{sec} \end{pmatrix} \tag{3.3.3}$$

C_{sec}, d_{sec}, A_{sec}, b_{sec} are the "original" vector and matrices of the specific section *sec* as described in section 2.2.2. So, with this solution it is sufficient to keep the temporal and zonal description of the system only in the bounds and constraints, and not in the objective function. Obviously, there is no control how the generators output power is distributed among the zones because there could be many ways of maximizing equation (3.3.1) and the solver chooses the one he "prefers". Moreover, this approach is very easy to implement starting from the "original" version, and the user can decide in which sections of the code to use it. Indeed it should not be used to perform the storage discharge because, as explained in section 2.2.2, in that case, it is very important to optimize the exploitation of the available energy through the forecast interval by distributing it according to the residual demand profile. A similar argument can also be made for energy-constrained dispatchable plants, but, as shown later in table 3.12, using *linprog* in this section instead of *lsqlin* does not have a significant impact on LCOTE or on the ability to meet the demand. Finally, the K_D coefficient cannot be used, so in case there is still unserved load at the end of the last section of the code (i.e. turbo-gas generators), it may happen that it is not distributed equally among the zones. This problem does not occur if the demand is completely covered.
S-3Z-Fus/RES, *S-Fus/RES* and *S-Fus/RES-3D* are used again to show the effects of this new formulation of dispatch optimization. In particular each scenario is simulated with three COMESE versions that differ according to the code sections in which *linprog* is implemented: in $linp_{noS,Hy}$ the storage discharge and *HyDam* sections are excluded from the modifications just explained, in $linp_{noS}$ only the storage discharge formulation is kept as in the original version and in $linp$ all the code sections are modified by moving from the *lsqlin* formulation to the *linprog* formulation. In each case, New charge1 is implemented.
From the results reported in table 3.12 it clearly emerges that:

- using *linprog* leads to a significant reduction in the computational time
- if the *linprog* formulation is implemented also in the storage discharge section, a general worsening in the LCOTE, E_{biogas} and $E_{unserved}$ (if present) appears in all the scenarios.
- if the *linprog* formulation is not implemented in the storage discharge and *HyDam*

		Original	$linp_{noS,Hy}$	$linp_{noS}$	$linp$
S-3Z-Fus/RES	time [s]	300	250	210	150
	LCOTE [c€/kWh]	10,14	10,14	10,14	10,19
	E_{biogas} [TWh]	33, 48	33, 48	33, 48	34, 67
	$E_{unserved}$ [TWh]	0	0	0	0
S-Fus/RES	time [s]	1100	770	560	340
	LCOTE [c€/kWh]	12,18	12,18	12,18	12,31
	E_{biogas} [TWh]	24, 16	24, 16	24, 16	26, 82
	$E_{unserved}$ [TWh]	0	0	0	0
S-Fus/RES-3D	time [s]	1210	880	640	450
	LCOTE [c€/kWh]	15,45	15,45	15,46	15,65
	E_{biogas} [TWh]	889, 4	889, 5	889, 9	913, 2
	$E_{unserved}$ [TWh]	150, 6	150, 6	151, 1	159, 1

Table 3.12: *linprog* and *lsqlin*: comparison of the results of test scenarios

section, the overall results do not change with respect to the original version.

- introducing *linprog* in the *HyDam* section has negligible impact on the final results. This is due to the fact, in the scenarios presented, the installed power of reservoir hydropower generators is very little compared to that of other technologies (for instance in *S-Fus/RES* the total nominal powers of *HyDam*, storage and biogas generators are respectively 10, 5GW, 175GW and 145GW.

Obviously, in scenarios with other characteristics, where, for example, reservoir hydropower plants cover a large share of the demand, it is necessary to analyze which is the impact of using *linprog* in the various sections of COMESE, so that the right trade-off between code speed and accuracy in the solution can be found. To sum up, this formulation is particularly suitable when using the DE optimization algorithm, because it allows an important reduction of the computational burden without greatly affecting the final results. Indeed, LCOTE, hours of unserved load, and total energy produced by biogas fired dispatchable generators remain essentially unchanged with respect to the "*lsqlin*" version, and the solutions that do not allow demand balancing are discarded by the optimizer. Once the optimal configuration of the generation park is identified, a more detailed model can be used to analyze the hourly operation of the obtained system. In the next chapter $linp_{noS}$ coupled with the differential evolution algorithm is used to study Italian decarbonization scenarios.

3.4 Economical model of the transmission grid

The LCOTE equation 2.3.1 is modified by adding Co_{grid} that takes into account the costs related to the transmission lines:

$$LCOTE = \frac{\sum_{i=1}^{i=N_p} (LCOE_i \cdot E_i) + Co_{stor} + Co_{grid}}{E_{load}} \tag{3.4.1}$$

Starting from the simplified grid model described in chapter 2, it is necessary to specify, as input parameters, the length *le* and the "type" of transmission line (over the head line, cable line...) for each interconnection between the zones. Then a maximum transmission capacity T_{Cl} is associated to each type of line, so that it is possible to compute the actual number of lines nl that form an interconnection of capacity T_C and the total number of lines in the system Nl:

$$nl_i = \frac{T_{C,i}}{T_{Cl,i}} \qquad N_l = \sum_{i=1}^{N_l} nl_i \tag{3.4.2}$$

For instance, nl for a overhead power line (*OHL*) is set to 2 GW, whereas it is reduced to 1 GW for high voltage cable lines. Finally, the number of substations in the system N_{ss} is calculated as follows: for OHLs, an average line length (le_{avg}) of 43 km is assumed, so that $N_{ss\,OHL} = le_{OHL}/le_{avg} + 1$; on the other hand, only the presence of a substation at the start and arrival of the line is considered in the case of cable lines. Usually, the cost for installing a line I_l and the relative operation and maintenance costs $O\&M_l$ are given per unit length (e/km), consequently, taking into account also the costs for decommissioning at the end of life, Co_{grid} is computed as:

$$Co_{grid} = \sum_{i=1}^{Nl} \left(I_{l,i} \frac{r(1+r)^{n_j}}{(1+r)^{n_j} - 1} \cdot l_i + O\&M_{l,i} \cdot l_i \right) + \sum_{j=1}^{Nss} I_{ss,j} \frac{r(1+r)^{n_j}}{(1+r)^{n_j} - 1} \tag{3.4.3}$$

where $I_{ss,j}$ is the investment cost needed for the j-th substation. Obviously, the presented model relies on some simplifications because each interconnection represents a set of transmission lines which actually could be very different from each other. If the technical and economical details of a interconnection are known in advance, it is possible to create an *ad hoc* cost file for that grid section and add its contribution to Co_{grid}. Anyway, it should be remembered that the LCOTE is an indicative economi-

cal parameter which is used to compare different scenarios rather than to forecast the future price of electricity.

3.5 Summary of main upgrades implemented in COMESE

This section briefly outlines the major modules introduced in COMESE, highlighting for each section its scope and its main effects on the code.

- **Transmission losses**. Introduction of transmission losses using an approximate linear model. Useful to perform a more detailed analysis on the role of the transmission grid. It must be coupled with a power flows minimization method (as described in section 3.1.1 and 3.1.2) and it leads to a strong increase in the computational burden.

- **New charge1**. Smarter storage charge operation which gives charging priority to the zones where is more difficult to balance the demand. Compatible with the presence of transmission losses. It leads to improvements in the final results (LCOTE, unserved demand, dispatchable generators energy output) especially in scenarios characterized by a high share of non-programmable energy sources and storage capacity, and significant grid constraints.

- **New charge2**. Linear programming formulation of storage charge, alternative to "New charge1". Compatible with the presence of transmission losses. In the scenarios where "New charge1" is more effective it can lead to a slightly worsening of the LCOTE. Significantly lower computational burden with respect to "New charge1".

- **New discharge**. Smarter storage discharge operation which gives discharging priority to the zones with higher overgeneration. Not compatible with the presence of transmission losses. It leads to improvements in the final results (LCOTE, unserved demand, dispatchable generators energy output) especially in scenarios characterized by a high share of non-programmable energy sources and storage capacity, and with impactful grid constraints.

- **New dispatch formulation**. It allows to move from a quadratic programming problem to a linear programming problem in each code section. Not compatible with the presence of transmission losses. Not recommended in the storage discharge section. It leads to a strong reduction in the computational burden without

(or little) affecting the overall results (LCOTE, generators energy output). Useful when coupling COMESE with the DE optimizer, not suitable for performing detailed analysis on the hourly operation of the various technologies.

- **Economical model of the transmission grid**. Integration in the LCOTE of the costs related to the transmission grid. Useful to evaluate the economical impact of the interconnections among the zones and to find the trade-off between additional connection capacity and generation capacity.

Chapter 4

Study of Italian decarbonized scenarios

As mentioned in the introduction of this thesis, challenging decarbonization targets have been set at both European and national levels, with the final aim to achieve carbon neutrality by 2050. Certainly, the power sector will be affected by profound changes due to an ever greater integration of non-programmable renewable power plants, which will have to be coupled to energy storage systems (presumably of electrochemical type).

This chapter presents an in-depth study of Italian decarbonization scenarios for the achievement of the net-zero emissions condition by the year 2050, in order to assess their techno-economical feasibility and the role that the transmission grid may have in contributing to achieve the challenging decarbonization goals. In particular two classes of scenarios are analyzed (*S-RES*, *S-Fus/RES*), which differ in the presence of fusion power plants. In fact, this type of base-load generation will enable power generation with very low greenhouse gas emissions and, unlike photovoltaic and wind power, it is not subject to the intermittency of natural phenomena and has high equivalent full-load working hours. Moreover, in recent years there has been a renewed interest in this technology, confirmed by numerous investments both in public research and private companies. Both the copper-plate and zonal analysis are carried out and a further study is proposed in order to evaluate which is the effect on the system behaviour of different PV and storage plants distribution. Finally, the scenarios are analyzed supposing different increments in the transmission capacity of the lines.

4.1 Techno-economical features of the scenarios

4.1.1 Long-term Italian electrical demand

As regards to the Italian electricity demand, reference is made to [30]: final energy consumption is supposed to decrease to 70 million tons of equivalent oil (toe) with respect to the current 120 mil. toe thanks to a gradual increase in energy efficiency and rational use of energy. On the other hand, the share of electricity in the final consumption will rise from about 20% to 55%, leading to a total demand of 650 TWh. This "electric revolution" affects also how energy is produced (as explained above), and used in the various sectors: the electric load profile will change both from a seasonal and daily point of view due to new kinds of consumption, in particular, the 100 TWh that are supposed to be allocated for the charging of electric vehicles will be predominantly required during the night hours [5]. Moreover, the requirements for residential, tertiary, and industrial heating will be concentrated in autumn and winter, and the 140 TWh dedicated to the production by about 3 million tons of green hydrogen, destined for hard-to-abate sectors, is considered a base-load over the whole year. The resulting demand profile has a peak of 145 GW at the end of January. In both *S-RES* and *S-Fus/RES*, Italy is modelled as composed by 6 zones and the electric load is allocated according to Terna data [25]: 55% North, 10% Centre-North 18% Centre-South, 9% South, 6% Sicily, 3% Sardinia.

4.1.2 Transmission grid model

To perform the simulation of the scenarios it was chosen to use the grid model described in the *Piano di Sviluppo 2021* by Terna [23], which takes into account the investments on grid expansion that the Italian TSO plans to realize in the next ten years. In particular, with respect to the current structure of the transmission grid, the interconnection among the zones is strengthened thanks to an overall increase in the transmission capacity and, most importantly, thanks to the "Tyrrhenian Link", a submarine high-voltage direct current cable line that will connect Sicily, Sardinia, and Campania (see figure 2.3). The transmission capacity of all the interconnections is shown in table 4.1 comparing the present values and the ones reported in [23]. In section 4.3 of this chapter a sensitivity analysis on possible future grid upgrades is carried out. In particular, three situations are considered where the values in table 4.1 are scaled by a factor x1, x2, x5 in order to better understand the impact of grid

Interconnection	present [GW]	*Pds2021* [GW]
N-CN	3,9	4,3
CN-CS	2,5	2,9
CN-Sar	1	1,1
CS-S	4,6	5,55
CS-Sic	–	0,7
CS-Sar	0,9	0,9
S-Sic	1,2	1,75
Sic-Sar	–	0,8

Table 4.1: Transmission capacity of interconnections among Italian zones: present situation and future development according to *Piano di Sviluppo 2021* (*PdS2021*).

constraints on the final results.

4.1.3 Generation and storage technologies

All the scenarios presented are based on of CO_2-free technologies, taking into account their foreseeable developments in the long run and the consequent costs. The main input parameters can be summarized as follow:

- The installed power and the yearly energy production of Geothermal (*Geo*), municipal solid waste (*MSW*) and run-of-the-river (*ROR*) power plants is fixed to the current values, which are summarized in table 4.2.

	Geo		*MSW*		*ROR*	
	P_n [MW]	h_e	P_n [MW]	h_e	P_n [MW]	h_e
N	—	—	125	7008	4400	4800
C-N	800	7884	40	7008	270	4100
C-S	—	—	18	7008	250	3130
S	—	—	26	7008	170	5220
Sic	—	—	—	—	150	3200
Sar	—	—	8	7008	140	3200

Table 4.2: Installed power and equivalent full-load working hours of *Geo*, *ROR* and *MSW* plants in each zone

- The hourly generation profile of the non-programmable renewable-source generators are taken from the TSO data [1]. In particular, 2015 is chosen as the reference

year because it is characterized by good availability of PV and wind generation, and it is also taken as reference year in numerous institutional scenarios [4], [29]. PV systems are divided into 3 categories: residential (*PVr*), industrial (*PVi*), and utility-scale (*PVu*). The last ones are supposed to be equipped with a mono-axial tracking system. Whaever the scenario, the PV technology share per zone is: 18% *PVr*, 48% *PVi*, and 34% *PVu*. The overall installed power is a variable that is set by the optimization algorithm, while its distribution among the zones is, at first, set proportional to the zonal demand. Table 4.3 presents, for each zone, the equivalent full-load working hours h_e of the various PV plants.

	h_e		
zone	*PVr*	*PVi*	*PVu*
N	1085	1300	1651
C-N	1183	1359	1744
C-S	1242	1394	1777
S	1323	1422	1833
Sic	1357	1503	1943
Sar	1241	1475	1917

Table 4.3: Equivalent full-load working hours of different PV plants in each zone

- The 2015 hourly generation profile of onshore wind (OnSW) power plants has been corrected so that the average capacity factor is 23%: this is due to the assumption that the development of this technology compensates for the use of sites with lower windiness. In fact, it is assumed that a total of 35 GW of wind power plants will be installed by 2050, keeping the current distribution among the zones. As regards to offshore floating wind farms (OffSW), the generation profile has been defined using a simulator [1], and the resulting average capacity factor is 35% (which is equivalent to about 3000 h_e). The installed power is an output of the optimization process, and, initially, it is equally divided among zones South, Sicily and Sardinia (see table 4.4).

- Two types of dispatchable generators are taken into account: water-reservoir hydropower plants (*HyDam*) and turbo-gas generators fired by biomethane (Bio-Gas). Suitable sites for the construction of *HyDam* are already fully exploited,

[1] see https://www.renewables.ninja/

	on-shore wind		off-shore wind	
	P_n [GW]	h_e	P_n [GW]	h_e
N	0,8	1250	?	1500
C-N	0,6	1600	?	2750
C-S	8	1900	?	2250
S	18	2000	?	3000
Sic	5	2100	?	3000
Sar	2,5	2400	?	3000

Table 4.4: Installed power and equivalent full-load working hours of wind power plants in each zone

consequently the installed capacity is set to 10 GW (2021 data) and the maximum available energy to an average value of 24 TWh. The optimization algorithm provides the installed power of BioGas generators, which is distributed among the zones following the demand distribution. Moreover, the maximum energy that can be produced by BioGas plants is limited to 45 TWh. Indeed, the highest value of bio-methane national potential reported in literature is 107 TWh [31], which translates into 45 TWh of maximum electric energy production when a 42% efficiency is considered.

- As regards to storage plants, the capacity of pumped hydro storage (PHS) systems is set to 12 GW taking into account future expected installations [14], for a total energy capacity equal to 0,12 TWh. Electrochemical storage (ES) is modelled considering utility-scale lithium batteries characterized by 8 hours of full-load capacity. The total installed power is defined by the optimization algorithm, and, at first, it is distributed among the zones proportionally to the electricity zonal load.

- *S-Fus/RES* considers also the presence of fusion power plants allocated following the load distribution. The optimal value of installed capacity is an output of the optimization process.

4.1.4 Economical characterization of the technologies

Table 4.5 summarizes the main economical parameters of the various technologies. The cost data of Geo, MSW as well as all hydro power plants are taken from the SETIS database [13]. The costs of PV systems and onshore wind power plants are as in the

Net Zero IEA scenario [19], while [9] is taken as reference for electrochemical storage systems. Finally, costs of future fusion power plants are taken from literature for a DEMO like tokamak plant [7]. The cost of transmission lines are implemented as

	CAPEX [€/kW]	OPEX [€/kWy]	lifetime [y]
Geo	3500	80	30
MSW	4500	140	25
ROR	3000	75	60
PV_r	450	12	25
PV_i	350	10	25
PV_u	350	12	25
OnSW	1300	30	25
OffSW	2200	70	25
HyDam	3400	70	60
BioGas[2]	550	20	15
PHS	1500	30	60
ES	960	20	10
fusion	5500	110	50

Table 4.5: Capital expenditure (CAPEX), operational expenditure (OPEX) and lifetime of the examined power plants

described in section 3.4. The data are taken from Terna [10] and ACER [11], and the values obtained are consistent with the ones reported in [33].

	CAPEX		OPEX [k€/($km \cdot y$)]	lifetime [y]
	lines [k€/km]	substation [k€]		
OHL	825	40000	29	40
HVDCc[3]	240	120000	8,4	40
HVACc[4]	5000	40000	60	40

Table 4.6: Economic parameters of transmission grid

[2]The cost of biomethane is set to 0.8 €/m^3; the efficiency of open-cycle biogas generators is set to 40%.

[3]High Voltage Direct Current cable line; submarine installation.

[4]High Voltage Alternating Current cable line; double circuit.

4.2 Copper-plate Analysis

This section presents the results obtained with the copper-plate approach, i.e. all the zones are gathered together in a single node as if the grid had infinite capacity. As explained above, the optimization algorithm looks for the configuration with the lowest LCOTE by varying four variables: the installed capacities of PV plants, BioGas generators, off-shore wind plants, and ES systems. In the case of *S-Fus/RES* also the rated power of fusion plants is set by the DE optimizer in a range from 0 to 60 GW. A solution is considered feasible only if the presence of unserved load does not exceed three hours. [27]. Table 4.7 summarizes the obtained overall installed capacity (P_n) and yearly energy generation (E_{gen}) of the main technologies. *PV* and *Hydro* take into account, respectively, all the photovoltaic (PV) systems (residential, industrial, utility scale) and all the hydro-power plants (run-of-the-river, water reservoir, pumped storage). Moreover, for each scenario the excess energy (E_{OG}), i.e. over-generation that needs to be curtailed, and the system cost are reported. It is apparent how the presence

	S-Fus/RES		*S-RES*	
	P_n [GW]	E_{gen} [TWh]	P_n [GW]	E_{gen} [TWh]
PV	140	201	640	910
OnSW	35	70	35	70
OffSW	0	0	10	30
Hydro	28	61	28	69
BioGas	43	41	46	45
fusion	60	420	0	0
ES	20	25	130	215
	Peak [GW]	Tot [TWh]	Peak [GW]	Tot [TWh]
E_{OG}	110	130	400	460
LCOTE	8,53 [c€/kWh]		10,2 [c€/kWh]	

Table 4.7: Results of copper-plate analysis

of fusion power plants has a positive impact on the cost of electricity, because it leads to a strong reduction in the needed PV and ES capacity. In fact the optimizer chooses to install 60 GW of fusion capacity, which is the maximum available value. In scenario *S-RES*, more than 600 GW of photovoltaic power is installed, so about 30 times the current value. Moreover, this leads to many periods of over-generation: the peak of

over-generation is almost 3 times the load maximum value, while the total energy that needs to be curtailed is 460 TWh, compared to 130 TWh of the *S-Fus/RES* case.

4.2.1 Changing the geographical distribution of renewable and storage systems

S-RES and *S-Fus/RES* assume that the photovoltaic generation as well as the new storage capacity will be allocated proportionally to the electricity load in the zones, i.e. mainly in the north of Italy. This paragraph presents the results obtained by changing the distribution of PV, wind, and ES systems. In particular, two alternatives are studied:

- Request-for-grid-connections distribution (RGCd): the capacity of PV, wind (both on-shore and off-shore) and ES system is distributed among the zones according to the request for grid connections, registered by the end of 2020, which have an accepted "Soluzione Tecnica Minima Generale" (General Minimum Technical Solution) [14]. Table 4.8 shows how, in this case, most non-programmable RES capacity is concentrated in the south of Italy, thus far from major consumption centers.

- Equivalent-full-load-working-hours distribution (EHd): the installed power of PV and wind (both on-shore and off-shore) plants is distributed among the zones proportionally to the equivalent full-load working hours of these technologies in the various zones. It is supposed that ES systems follow the same distribution as PV plants. The resulting values are halfway between the original and RGC distribution: the share of installed capacity is slightly higher in the south of Italy and in the islands, but it is not such unbalanced as in the RGCd case.

Table 4.9 reports the obtained results: also in these cases fusion capacity reaches the maximum value and all the considerations made for *S-Fus/RES* and *S-RES* remain valid. It is interesting to note that the request-for-grid-connections distribution leads to power systems with lower LCOTE, especially in the full-renewables scenario. This is due to the fact PV and wind generators are installed mainly in the zones with higher capacity factors: in fact, the optimizer prefers to increase the installed capacity of PV (it grows from 520 GW in the EHd case to 580 GW) so as to reduce the rated power of BioGas and ES plants, which are characterized by relatively high capital costs. It is important to point out that this model does not take grid constraints into account, as well as the investments required to transmit the energy produced in the different zones of Italy. As will be shown below, this simplification can lead to misleading results,

	PV		on-shore wind		off-shore wind		*ES*	
	RGCd	EHd	RGCd	EHd	RGCd	EHd	RGCd	EHd
N	7,7	15	1,6	11	17	10	8,0	15
CN	2,7	16	2,6	14	0	18	1,0	16
CS	12	17	19	18	0	15	12	17
S	41	17	54	18	8,0	19	31	17
Sic	28	18	14	18	66	19	34	18
Sar	8,6	17	8,6	21	9,0	19	14	17

Table 4.8: Share (%) of installed capacity of PV, wind and ES plants according to RGCd and EHd

	S-Fus/RES-RGCd		*S-RES-RGCd*		*S-Fus/RES-EHd*		*S-RES-EHd*	
	P_n [GW]	E_{gen} [TWh]	P_n [GW]	E_{gen} [TWh]	P_n [GW]	E_{gen} [TWh]	P_n [GW]	E_{gen} [TWh]
PV	210	330	580	900	155	240	520	800
OnSW	35	71	35	71	35	68	35	68
OffSW	0	0	10	27	0	0	10	24
hydro	28	56	28	64	28	60	28	60
BioGas	33	32	44	45	36	33	47	45
fusion	60	420	0	0	60	420	0	0
ES	33	40	121	217	29	36	164	228
	Peak [GW]	Tot [TWh]	Peak [GW]	Tot [TWh]	Peak [GW]	Tot [TWh]	Peak [GW]	Tot [TWh]
E_{OG}	132	167	396	411	120	155	350	296
LCOTE	8,36 [c€/kWh]		9,56 [c€/kWh]		8,40 [c€/kWh]		10,1 [c€/kWh]	

Table 4.9: Copper plate analysis: results of RGC and EH distribution

particularly when the share of RES and ES systems in the zones does not reflect the electricity demand distribution. Indeed, the structure of the Italian power system is characterized by the fact that the load is concentrated mainly in the northern regions, but the producibility of photovoltaic and wind plants is greater in the south and in the islands. Anyway, even assuming that renewable source plants are installed in the most favorable sites and that the grid has infinite transmission capacity, a huge amount of photovoltaic plants would need to be installed, exceeding even the estimate reported in [30]. Instead, the presence of technology capable of covering the baseload demand without emitting greenhouse gasses (such as fusion) would make it easier, both from a technical and an economical point of view, to achieve the complete decarbonization of the system.

4.3 Zonal Analysis

In this section *S-Fus/RES* and *S-RES* are analyzed introducing the transmission grid model and the relative costs as explained in the former paragraphs. It was verified that the DE optimizer converges to the same solutions both with the "*linprog*" and "*lsqlin*" versions of the code (see chapter 3). So, to reduce the computational time, the optimization was carried out using the linear formulation of the dispatch model.
In order to move from the copper plate approach to the actual structure of the grid described by Terna in [23] (*PdS2021* scenarios), two intermediate cases are studied. First, the values of transmission capacity reported in table 4.1 are increased by five times (*x5* scenarios), thus reducing a lot the constraints on power exchanges among the zones. Then the same values are doubled (*x2* scenarios). It should be noted that the optimizer only chooses the total installed capacities of the selected technologies (PV, ES, OffSW, BioGas, and fusion), whereas their allocation among the zones is set by the user. The three distributions of RES and ES systems explained above are compared for each grid model.

4.3.1 *x5* scenarios

Table 4.10 shows, for each scenario, the LCOTE and the installed capacity of the technologies involved in the optimization process. The total costs associated to the interconnection among the zones, which are computed as explained in 3.4, amount to about $Co_{grid} = 2,9$ bil€. Therefore, the grid contribution to the LCOTE can be obtained by dividing Co_{grid} by the total electric demand, which results in 0,45 c€/kWh. The

	PV	ES	OffSW	Fusion	BioGas	LCOTE
S-Fus/RES	120	27	0	60	38	9,05
S-RES	690	140	10	0	47	11,1
S-Fus/RES-RGCd	185	35	2,5	60	32	8,96
S-RES-RGCd	–	–	–	–	–	–
S-Fus/RES-EHd	155	30	5	60	37	9,01
S-RES-EHd	850	158	0	0	46	11,9

Table 4.10: *x5* scenarios: optimal installed capacities [GW] and LCOTE [c€/kWh].

values relative to *S-RES-RGCd* are not reported because the optimizer wasn't able to find a feasible solution: even when the capacities of PV and ES are set to their maximum

available values (respectively 1000 GW and 350 GW), the energy required from BioGas generators greatly exceeds the 45 TWh limit. If the system is forced not to overcome 45 TWh of BioGas generation, no solution is able to balance the demand. Indeed the full-renewables scenarios are the ones mainly affected by the introduction of the grid model: *S-RES* has the capacity distribution that leads to the lower system cost, and the LCOTE of *S-RES-EHd* increases of about 20% with respect to the copper-plate analysis. On the other hand, the results of the scenarios that consider the presence of fusion power plants do not differ much from the ones obtained with the copper plate approach. Fusion capacity always reaches 60 GW, and RCG is confirmed to be the best distribution, although the LCOTE of *S-Fus/RES* and *S-Fus/RES-EHd* is not so different. Moreover, the presence of grid constraints does not affect much the system cost: if Co_{grid} is neglected the LCOTE increases by about 1% with respect to the values reported in table 4.9.

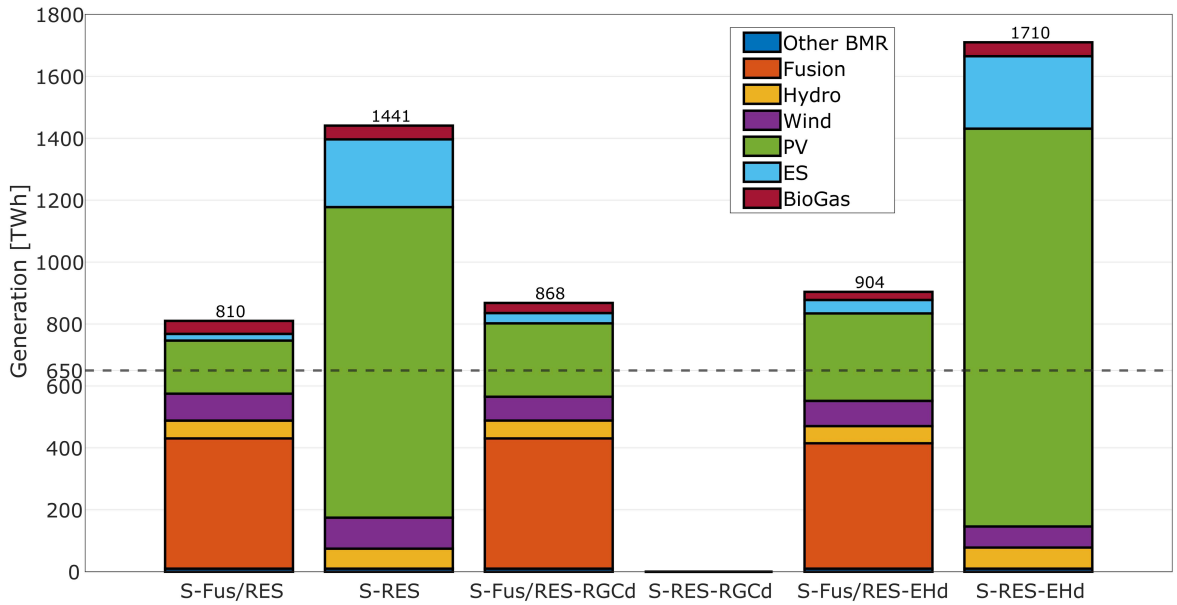

Figure 4.1: *x5* scenarios: total generation by technology. The dotted line corresponds to the total electricity demand

Figure 4.1 shows the yearly energy generated by each technology per scenario. The dotted line corresponds to the total electricity demand. It is apparent that the presence of fusion, in addition to lowering the cost of the system, leads to a huge reduction in the share of curtailed energy generation.

Optimal distribution of PV and storage plants

In the presented analysis the optimizer identifies the total capacity of "target" technologies, but the actual installed power in each zone depends on which distribution is chosen. In this section, the algorithm is free to vary the capacity of PV and ES systems in each zone, so as to find which is the optimal distribution. The starting point is the x5 scenarios studied above. In particular, in *S-Fus/RES* OffSW is fixed to 0 and fusion capacity to 60 GW, while in *S-RES* $OffSw = 10$ and $Fusion = 0$. The optimizer sets also the total BioGas capacity, but its distribution is fixed to the load-based distribution (as done in all the other simulations). Table 4.11 reports the total capacity (Tot) of

	S-Fus/RES			*S-RES*		
	PV	ES	BioGas	PV	ES	BioGas
N	12	10	55	42	44	55
CN	5,2	5,0	10	11	10	10
CS	9,8	10	18	21	26	18
S	43	34	9	15	10	9
Sic	21	27	6	8,8	7,8	6
Sar	9	14	3	2,2	2,2	3
Tot [GW]	145	25	36	670	130	47
LCOTE [c€/kWh]	8,62			10,5		

Table 4.11: Optimal distribution: share (%) of installed capacity of PV, ES and BioGas plants.

PV, ES and BioGas plants as well as its allocation among the zones. The presence of fusion power plants has a strong impact on the optimal distribution of PV and storage systems. Indeed, in *S-Fus/RES*, a large share of the baseload power generation in the various zones relies on fusion plants, giving the possibility to install photovoltaic capacity in the zones characterized by higher producibility. The resulting distribution is quite similar to RGCd. Consistently with the results in table 4.10, if fusion is removed PV and ES capacities have to be shifted mainly to the North zone, which accounts for more than half of the total demand. However, due to the high transmission capacity of the interconnections, in *S-RES* the share of PV and storage capacity in southern zones is higher than in the load-proportional distribution, leading to a slight decrease in the LCOTE.

4.3.2 *x2* scenarios

Table 4.12 reports, for each scenario, the LCOTE and the installed capacity of the technologies involved in the optimization process. The total costs associated to the interconnection among the zones amount to about $Co_{grid} = 1,2$ bil€. Therefore, the grid contribution to the LCOTE results in 0,18 c€/kWh.

	PV	ES	OffSW	Fusion	BioGas	LCOTE
S-Fus/RES	170	35	0	60	32	8,82
S-RES	715	150	7,5	0	54	11,2
S-Fus/RES-RGCd	185	32	2	60	59	9,45
S-RES-RGCd	–	–	–	–	–	–
S-Fus/RES-EHd	170	25	0	60	45	8,97
S-RES-EHd	–	–	–	–	–	–

Table 4.12: *x2* scenarios: optimal installed capacities [GW] and LCOTE [c€/kWh]

.

Compared with the *x5* scenarios, the effect of the distribution of renewables and storage capacity on the final results is more pronounced. In particular, the load-based distribution becomes the best in terms of system cost and, as regard to full-renewables scenarios, only *S-RES* leads to a feasible solution, while *S-RES-RGCd* and *S-RES-EHd* fail to respect the constraint on the maximum generation from BioGas plants. Moreover, the LCOTE increases only for *S-Fus/RES-RGCd*, whereas for the other scenarios it is more convenient to reduce the transmission capacities of the interconnections. As expected the grid plays an important role only when there is a pronounced unbalancing between demand and generation distribution.

Once again, scenarios with fusion generation present significantly better results, for instance the LCOTE decreases by 15%, and the total over-generation drops from 810 TWh to 275 TWh when comparing *S-RES* with the worst fusion-based scenario (*S-Fus/RES-RGC*).

In each scenario the electric energy generated from BioGas is close to 45 TWh, but the BioGas rated power varies a lot. Moving from a load-based distribution to the RGC distribution of renewables and electrochemical storage, the needed capacity of turbogas generators nearly doubles. This means that it is more difficult to balance demand peaks with just BMR and storage systems.

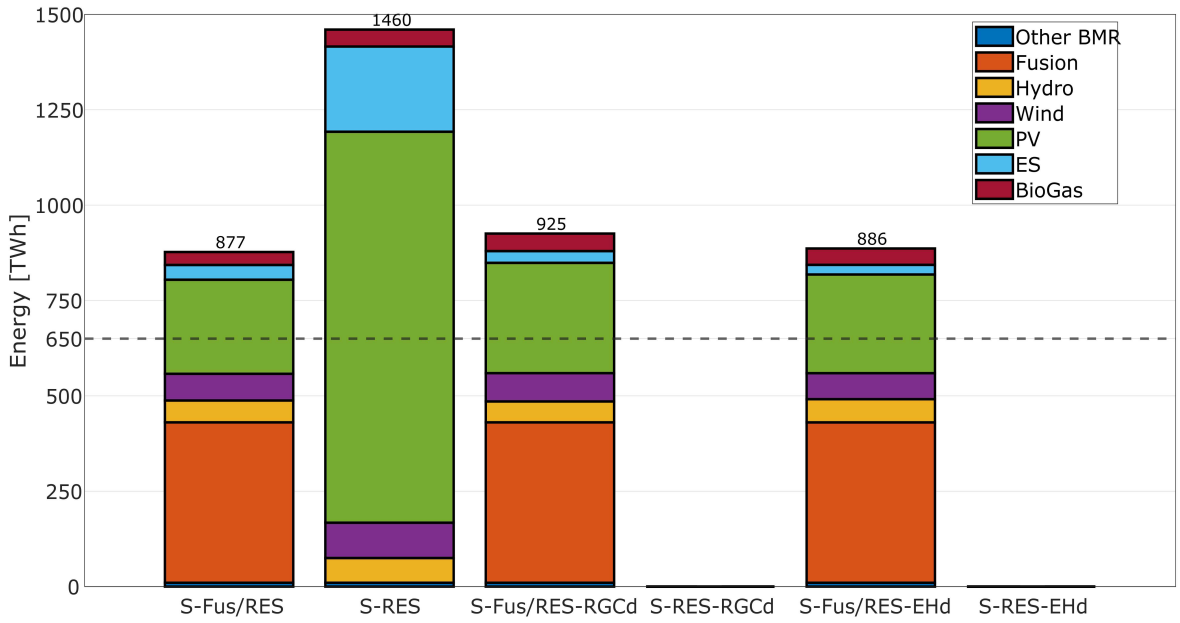

Figure 4.2: *x2* scenarios: total generation by technology

Optimal distribution of PV and storage plants

As done previously, also for the *x2* scenarios the DE optimizer is used to identify the optimal distribution of PV and storage plants starting from the capacity values reported in table 4.12. The obtained results are shown in table 4.13, which reports the

	S-Fus/RES			*S-RES*		
	PV	ES	BioGas	PV	ES	BioGas
N	47	48	55	60	55	55
CN	15	20	10	10	14	10
CS	14	11	18	11	11	18
S	16	19	9	13	14	9
Sic	6,3	1,3	6	4,1	5,4	6
Sar	1,7	0,7	3	1,9	0,6	3
Tot [GW]	155	25	37	700	135	53
LCOTE [c€/kWh]	8,77			10,8		

Table 4.13: Optimal distribution: share (%) of installed capacity of PV, ES and BioGas plants.

total capacity (Tot) of PV, ES and BioGas plants as well as its allocation among the zones. As regard to *S-Fus/RES*, the optimal distribution is significantly different from the *x5* case, meaning that the reduction in interconnection capacity has a strong impact on the

behavior of the entire system. The optimizer concentrates PV and storage capacity in high-demand zones, and this is even more pronounced in the full-renewables scenario. However, the advantages in terms of cost reduction are not so relevant. It is interesting to note that, with respect to the load-distribution case, in *S-Fus/RES* the optimal solution is characterized by an important decrease in ES capacity (-25%) but the BioGas nominal power increases from 32 GW to 37 GW. Although beyond the scope of this thesis, these results suggest that further investigations should be made in order to identify the optimal trade-off between storage and dispatchable generators capacity, also taking into account how these technologies are allocated among the zones.

4.3.3 *PdS2021* scenarios

Table 4.10 reports, for each scenario, the LCOTE and the installed capacity of the technologies involved in the optimization process. The total costs associated to the interconnection among the zones amount to about $Co_{grid} = 0,6$ bil€. Therefore, the grid contribution to the LCOTE results in 0,09 c€/kWh.

	PV	ES	OffSW	Fusion	BioGas	LCOTE
S-Fus/RES	170	34	0	60	33	8,80
S-RES	750	150	10	0	59	11,4
S-Fus/RES-RGCd	460	79	0	60	59	11,8
S-RES-RGCd	–	–	–	–	–	–
S-Fus/RES-EHd	215	32	0	60	53	9,47
S-RES-EHd	–	–	–	–	–	–

Table 4.14: *PdS2021* scenarios: optimal installed capacities [GW] and LCOTE [c€/kWh].

The results are consistent with what was observed for the *x2* scenarios and they underline the importance of performing the zonal analysis. With the *PdS2021* grid model, which implies the use of lower values of interconnection capacities with respect to the former simulations, it is apparent that placing the generation capacity in the high-load zones has a strong impact on the system behaviour. *S-Fus/RES* is by far the scenario with the lowest LCOTE and it is interesting to note that *S-RES*, where fusion is absent, has a lower system cost than *S-Fus/RES-RGCd*, where there are 60 GW of fusion capacity, but PV and ES plants are placed mainly in the south if Italy.
Table 4.15 present a comparison between the copper-plate and *PdS2021* scenarios by showing the percentage variations of the variables set by the DE optimizer. In Δ_{LCOTE}

the LCOTE values of the *PdS2021* scenarios are adjusted by removing the grid contribution, which is absent in the copper-plate analysis. All the percentage variations are computed using the values obtained in the copper plate case as reference, for instance:

$$\Delta_{PV} = 100\frac{PV_{PdS} - PV_{copper-plate}}{PV_{copper-plate}} \tag{4.3.1}$$

The scenario with the largest increases both in installed capacities and LCOTE is *S-Fus/RES-RGCd*, which is the one with the best performance in the copper-plate case. On the other hand, the presence of grid constraints do not affect much *S-Fus/RES*, which is characterized by a high share of constant baseload generation thanks to 60 GW of fusion capacity distributed among the zones proportionally to the zonal demand. As expected, *S-RES-RGCd* and *S-RES-EHd* do not lead to any feasible solution. For instance, even assuming $P_{n\,PV} = 1000GW$ and $P_{n\,ES} = 350GW$, *S-RES-RGCd* would need 200 TWh of BioGas generation to guarantee demand balancing. Similarly, the unserved load increases to 150 TWh when the system is imposed to not overcome 45 TWh of BioGas generation. This is due to an unfavorable distribution of PV and ES capacity, and to the presence of interconnections with finite transmission capacity. Figure 4.4 shows the number of congestion hours per interconnection, distinguishing positive and negative power flows. The orientation assigned to each line is specified by its name, for instance the interconnection N-CN starts in zone North and end in zone Centre North. It is apparent that the system "tries" to move the generated energy from the south to the north of Italy, but transmission capacity is insufficient and so interconnections experience many hours of congestion. In particular, the CentreNorth-CentreSouth and CentreNorth-Sardinia interconnections seem to be the bottlenecks.

	Δ_{PV}	Δ_{Es}	Δ_{OffSW}	Δ_{Fusion}	Δ_{BioGas}	Δ_{LCOTE}
S-Fus/RES	21	70	0	0	-20	2
S-RES	20	15	0	0	29	9
S-Fus/RES-RGCd	110	58	0	0	72	41
S-RES-RGCd	–	–	–	–	–	–
S-Fus/RES-EHd	39	10	0	0	47	12
S-RES-EHd	–	–	–	–	–	–

Table 4.15: Comparison of copper-plate and *PdS2021* grid model: percentage variations of installed capacities and LCOTE

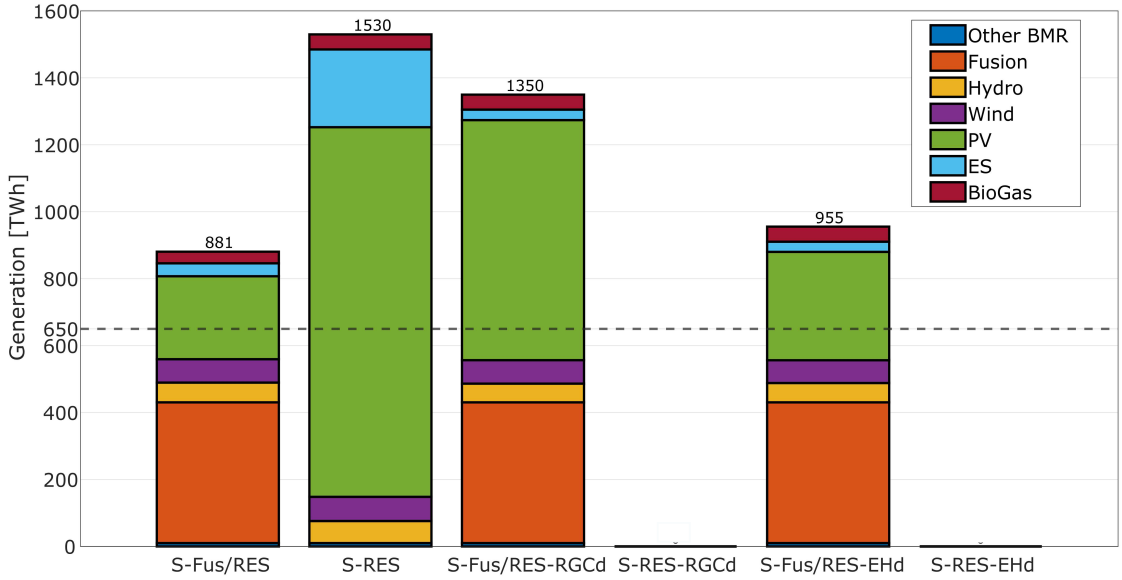

Figure 4.3: *PdS2021* scenarios: total generation by technology

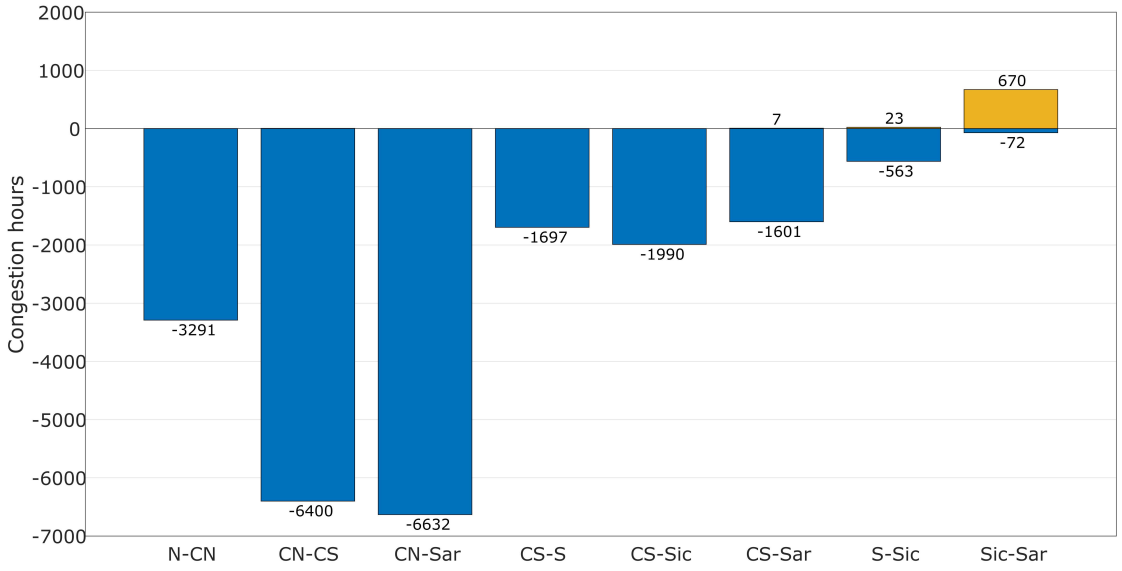

Figure 4.4: *S-RES-RGCd*, congestion hours. Negative hours refers to negative power flows

Optimal distribution of PV and storage plants

Table 4.16 reports the share of PV, ES and BioGas capacity per zone, as well as the respective cumulative values resulting from the optimization of the distribution of photovoltaic and storage systems. Consistently with the previous results, the optimal allocation of photovoltaic and storage capacity among the zones is quite similar to the load-based distribution. Actually, even more capacity is shifted from the island to the

	S-Fus/RES			*S-RES*		
	PV	ES	BioGas	PV	ES	BioGas
N	59	59	55	61	57	55
CN	14	18	10	14	17	10
CS	11	11	18	11	11	18
S	11	11	9	8,5	11	9
Sic	3,4	0,9	6	3,9	3,8	6
Sar	1,5	0	3	1,9	0,9	3
Tot [GW]	160	30	31	710	140	57
LCOTE [c€/kWh]	8,61			11,0		

Table 4.16: Optimal distribution: share (%) of installed capacity of PV, ES and BioGas plants.

norther zones. This is particularly evident for *S-Fus/RES*, where storage capacity is nearly completely removed from Sardinia and Sicily.
These considerations hold also for *S-RES*. With respect to the load-based distribution, the optimal distribution slightly increases the share of photovoltaic and storage capacity in the northern zones by reducing the installed power in Sicily and Sardinia. This lead to a reduction in the required total capacity of PV, ES plants by, respectively, 40 GW and 10 GW. Also the LCOTE decreases by about 4%.
The presented analyses prove how the distribution of photovoltaic and storage capacities among the zones, together with the transmission capacity of interconnections, are crucial to determining the optimal operation of the power system and strongly influence the final outcomes of the scenarios. Figure 4.5 summarizes the most important considerations. For *x5* and *x1* cases, it shows the optimal distribution of PV capacity, which is quite similar to the ES optimal distribution, regarding both the full-renenwables and fusion plus renenwables scenarios. It is convenient to install PV capacity mainly in the south of Italy (where the capacity factor is higher) only if transmission grid capacity is greatly increased, and only if there is the presence of a high share of baseload generation, provided by fusion power plants, distributed proportionally to the zonal electricity demand. In all the other cases the share of PV (and electrochemical storage) capacity is significantly higher in the northern zones. This is particularly evident for the *x1* RES scenario where the Nord and Centre-Nord zones account for the 75% of the overall photovoltaic capacity, and this share is even higher if ES capacity is included. It is important to note that this distribution is contrary to the current trend of request for grid connections of RES and storage plants reported by Terna.

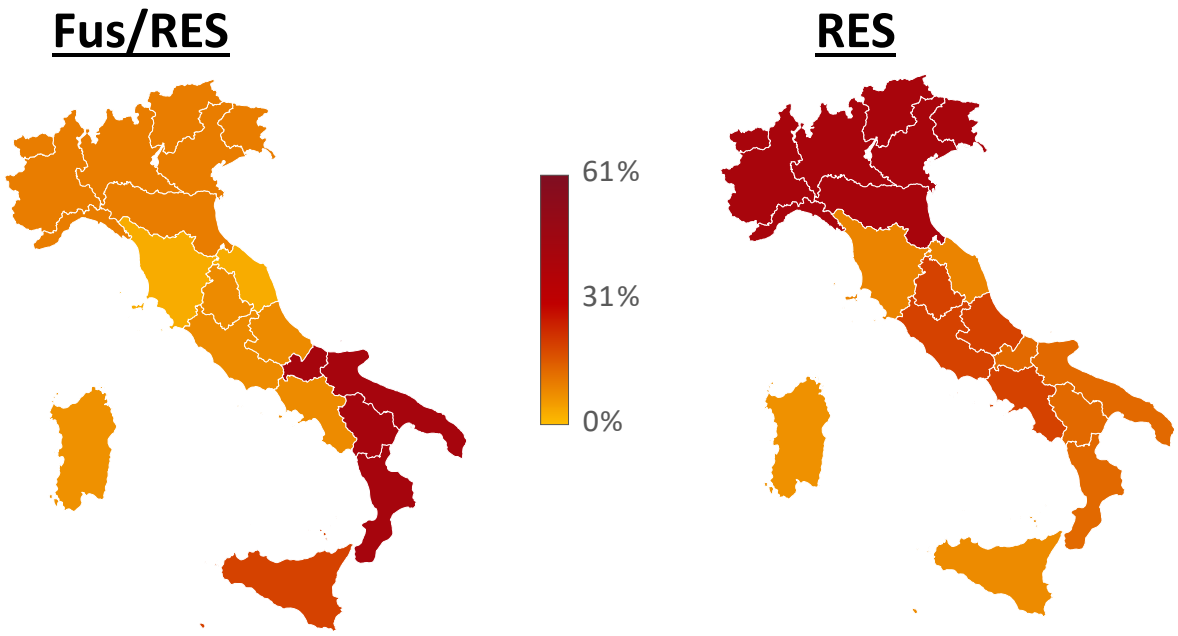

(a) Share [%] of installed PV capacity. *x5* scenarios

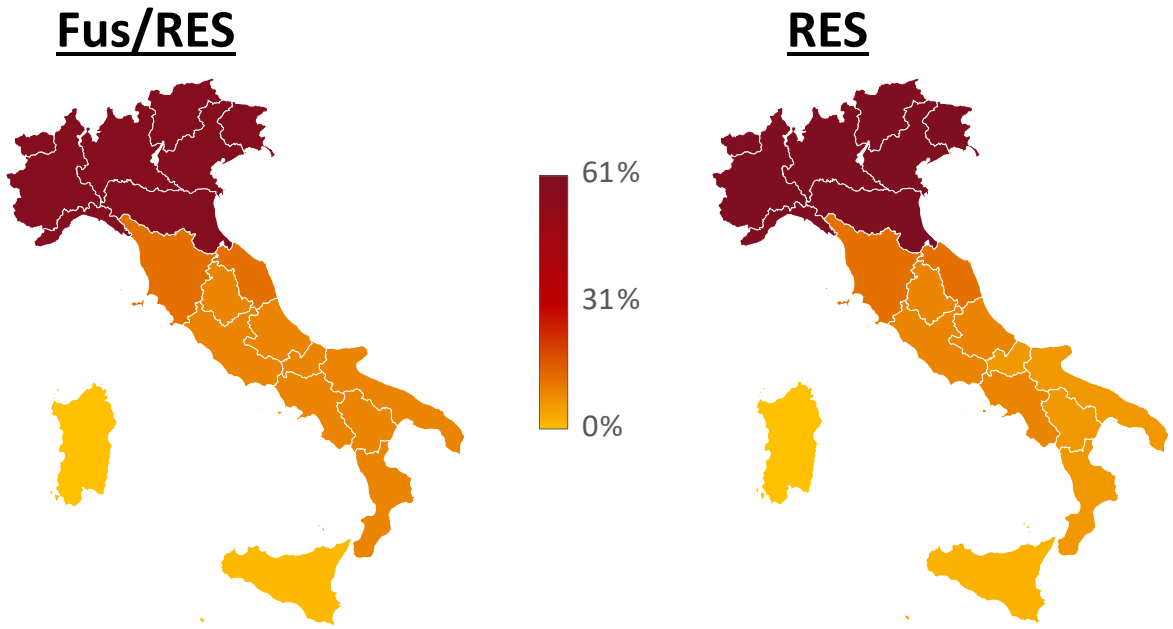

(b) Share [%] of installed PV capacity. *x1* scenarios

Figure 4.5: Optimal distribution of PV capacity. *x1* and *x5* scenarios

Chapter 5

Conclusions and Future Works

The EU aims to be the first carbon-neutral continent by 2050, and its member states are adopting challenging decarbonization policies in order to reach this important goal. In particular, the power sector will undergo a radical transformation both from the supply and demand point of view. The electricity mix will present a high share of non-programmable sources and the load curve is expected to grow significantly due to greater electrification of final consumption. Therefore it is important to have a tool capable of assessing the techno-economical feasibility of carbon-neutral scenarios and pointing out the strengths and weaknesses of different decarbonization strategies.

The COMESE code performs an hourly simulation of the power sector, which is needed to properly evaluate the behaviour of storage systems and dispatchable generators. Moreover, it allows to take into account the constraints due to the presence of the transmission grid. As described in chapter 3 the grid model has been further improved, introducing an economical characterization of transmission lines, transmission losses, and the possibility to choose the rationale behind grid management (for instance minimizing the power exchanges between the nodes). Also the storage section has been modified through the implementation of alternative approaches to perform a "smarter" charge and discharge. In particular, they are effective only when the zonal analysis is carried out and grid constraints greatly affect the system behaviour.

It has been verified that, for the scenarios under analysis, these modifications lead to slight improvements in the quality of final results, but it is preferable to choose a simplified model to reduce the computational burden, especially when performing the optimization of the power sector configuration. Indeed, if the dispatchment is formulated as a linear programming problem the running time drastically decreases, which is an important advantage when coupling the code with the DE optimizer. This is exactly

what has been done in chapter 4 in order to study several Italian decarbonized scenarios. The analysis focused on the role of the transmission grid, and on the impact of fusion generation on the system costs. It has been highlighted that the copper-plate approach can produce misleading results, and it is not adequate to evaluate the feasibility of decarbonization scenarios especially when the generation capacity is installed far from the high-load zones. When grid constraints are taken into account, the distribution of renewables and storage capacity has a strong impact on the system behaviour. The analyses have been performed introducing the transmission grid structure planned by Terna in "Piano di Sviluppo 2021" [23], and the results show that allocating PV and *ES* capacity proportionally to the load in each zone is close to the optimal distribution in terms of LCOTE. If PV and *ES* systems are installed mainly in the south of Italy (following the current trend [14]), major investments in grid expansion will be needed both to ensure demand balancing and to reduce the overall system cost.
In any studied scenario the presence of fusion, which is a constant baseload power source, has a positive impact on the final results. Indeed, when compared to full-renewables scenarios, the scenarios which allow the presence of fusion capacity are characterized by:

- Reduction in the required transmission capacity to guarantee demand balancing. .
- Considerable reduction in the necessary PV and storage capacity (about 4-5 times less). Also the dispatcahble generation capacity decreases
- Considerable reduction in the overgeneration. In full-renewables scenarios more than half of the total generated energy needs to be curtailed.
- Reduction in the LCOTE of more than 20%

In addition, the issues related to grid stability were not taken into account in these studies. Also from this point of view, the presence of fusion power plants would be favorable because it would increase the inertia of the system.

5.1 Future works

The presented analysis has underlined the importance of dispatchable generators to cover the demand peaks that cannot be balanced using *BMR* and storage systems.

Therefore it may be important to increase the degree of detail with which these technologies are modeled in the code. During the thesis work it has been tried to add ramp-up and ramp-down constraints, i.e. limit the derivative of the hourly profile of the generated power. Unfortunately, both the *lsqlin* and *linprog* formulations do not work properly when this constraint is added. Indeed, a significant aspect is that COMESE is written having as first aim the balancing of the demand, and the logic by which it tries to reach this goal is set "a priori", on the basis of assumptions on what could be the most sensible operation of the system. So, the unit commitment of the various technology, the management of storage devices and grid capacity, the mid-analysis section and so on are implemented following a pre-defined logic which, however sensible and justified may be, is not necessarily the best (or the most realistic). Moreover, this fact can lead to an increase in code complexity and has some limitations. An alternative approach could be setting a cost for the unserved load, in order to impose as objective function the total system cost (and not computing it a posteriori). In this way, the optimal dispatchment is set at once by the solver, which follows this new logic.
Finally, the COMESE code performs an hourly simulation of the power sector relying on the assumption that the hourly profile of load and renewable production over a user-defined future timeframe can be perfectly forecasted. This strong hypothesis is unlikely to be verified in future energy systems characterized by an important share of non-programmable generators and high varying electricity demand. Therefore, another possible development is the adoption of a stochastic approach, designed to account for the uncertainty and possible errors that can characterize forecasts of demand and especially of generation from intermittent sources, so as to assess the reliability of the simulated system as a function of the forecast quality.

References

[1] ENTSO-E. URL: https://transparency.entsoe.eu/.

[2] *A European Green Deal*. European Commission. 2019. URL: https://ec.europa.eu/info/strategy/priorities-2019-2024/european-green-deal_en.

[3] Herbst A. et al. "Introduction to Energy Systems Modelling". In: *Swiss Journal of Economics and Statistics* (2012). URL: https://link.springer.com/content/pdf/10.1007/BF03399363.pdf.

[4] *Baseline scenario of the heating and cooling demand in buildings and industry in the 14 MSs until 2050*. European Project. 2017. URL: https://heatroadmap.eu/wp-content/uploads/2018/11/HRE4_D3.3andD3.4.pdf.

[5] M. Benini et al. *Limpatto degli scenari di diffusione di PEV/PHEV sul sistema energetico nazionale e sulla rete di media e bassa tensione*. RSE report. 2011.

[6] M. Borasio and S. Moret. "Deep decarbonisation of regional energy systems: A novel modelling approach and its application to the Italian energy transition". In: *Renewable and Sustainable Energy Reviews* 153 (2022). DOI: https://doi.org/10.1016/j.rser.2021.111730.

[7] Bustreo C. et al. "How fusion power can contribute to a fully decarbonized European power mix after 2050". In: *Fusion Engineering and Design* 146 (2019), pp. 2189–2193. DOI: https://doi.org/10.1016/j.fusengdes.2019.03.150..

[8] *CO2 Emissions*. Our World in Data, website. URL: https://ourworldindata.org/co2-emissions.

[9] Wesley Cole, A. Will Frazier, and Chad Augustine. *Cost Projections for Utility-Scale Battery Storage: 2021 Update*. NREL. 2021. DOI: https://dx.doi.org/10.2172/1786976.

[10] *Documento Metodologico per l'applicazione dell'analisi costi benefici al Piano di Sviluppo 2021*. Terna. 2021. URL: https://download.terna.it/terna/Documento_Metodologico_applicazione_analisi_costi_benefici_applicata_Piano_Sviluppo_2021_8d940b13ac09317.pdf.

[11] *Electricity Infrastructure Unit Investment Costs*. ACER. 2015. URL: https://www.acer.europa.eu/Official_documents/Acts_of_the_Agency/Publication/UIC%5C%20Report%5C%20%5C%20-%5C%20Electricity%5C%20infrastructure.pdf.

[12] *Energy Production and Consumption*. Our World in Data, website. URL: https://ourworldindata.org/energy-production-consumption%22.

[13] *ETRI 2014 - Energy Technology Reference Indicator projections for 2010-2050*. Publications Office of the European Union. 2014. URL: https://publications.jrc.ec.europa.eu/repository/handle/JRC92496.

[14] *Evoluzione rinnovabile - Piano di Sviluppo 2021*. Terna. 2021. URL: https://download.terna.it/terna/Evoluzione_Rinnovabile_8d940b10dc3be39.pdf.

[15] Roger A. Horn and Charles R. Johnson. *Matrix Analysis*. Theorem 7.2.7. Cambridge University Press, 2013.

[16] *Individuazione Zone della Rete Rilevante*. Terna. 2021. URL: https://download.terna.it/terna/0000/1142/92.PDF.

[17] Després J. et al. "Modelling the impacts of variable renewable sources on the power sector: Reconsidering the typology of energy modelling tools". In: *Energy* (2015). DOI: https://doi.org/10.1016/j.energy.2014.12.005.

[18] J. Lampinen. "A constraint handling approach for the differential evolution algorithm". In: 2 (2002), 1468–1473 vol.2. DOI: 10.1109/CEC.2002.1004459.

[19] *Net Zero by 2050*. IEA. 2021. URL: https://www.iea.org/reports/net-zero-by-2050.

[20] Fabian Neumann, Veit Hagenmeyer, and Tom Brown. "Assessments of linear power flow and transmission loss approximations in coordinated capacity expansion problems". In: *Applied Energy* 314 (May 2022), p. 118859. DOI: 10.1016/j.apenergy.2022.118859.

[21] *Optimization Toolbox User's Guide*. MathWorks. 2022. URL: https://www.mathworks.com/help/pdf_doc/optim/optim.pdf.

[22] Tozzi P. and Jin Ho Jo. "A comparative analysis of renewable energy simulation tools: Performance simulation model vs. system optimization". In: *Renewable and Sustainable Energy Reviews* 80 (2017), pp. 390–398. DOI: https://doi.org/10.1016/j.rser.2017.05.153.

[23] *Piano di Sviluppo 2021*. Terna. 2021. URL: https://download.terna.it/terna/Piano_Sviluppo_2021_8d94126f94dc233.pdf.

[24] *Piano nazionale integrato energia e clima (PNIEC)*. Mise,Italian Government. 2019. URL: https://www.mise.gov.it/images/stories/documenti/PNIEC_finale_17012020.pdf.

[25] *Pubblicazioni Statistiche*. Terna. 2021. URL: https://www.terna.it/it/sistema-elettrico/statistiche/pubblicazioni-statistiche.

[26] Storn R. and Price K. "Differential Evolution A Simple and Efficient Heuristic for Global Optimization over Continuous Spaces". In: *Journal of Global Optimization* (1997). DOI: https://doi.org/10.1023/A:1008202821328.

[27] *Rapporto Adeguatezza Italia 2021*. Terna. 2021. URL: https://download.terna.it/terna/Terna_Rapporto_Adeguatezza_Italia_2021_8d9a51d27ad741c.pdf.

[28] *Statistical Review of World Energy- all data*. Available online. BP. 2021. URL: https://www.bp.com/en/global/corporate/energy-economics/statistical-review-of-world-energy.html.

[29] *Strategia energetica nazionale (SEN)*. Mite, Italian Government. 2017. URL: https://www.mise.gov.it/images/stories/documenti/Testo-integrale-SEN-2017.pdf.

[30] *Strategia italiana di lungo termine sulla riduzione delle emissioni dei gas a effetto serra*. Mite, Italian Government. 2021. URL: https://www.mite.gov.it/sites/default/files/lts_gennaio_2021.pdf.

[31] S. Teske, T. Morris, and K. Nagrath. *100% Renewable Energy: An Energy [R]evolution for ITALY*. Report prepared by ISF for Greenpeace Italy. 2020. URL: https://www.greenpeace.org/static/planet4-italy-stateless/2020/06/a7955fe1-italy-report-forgp-2020.pdf.

[32] *User Guide - Optimal Power Flow*. Plexos. 2021.

[33] Zappa W., Junginger M., and van den Broek M. "Is a 100% renewable European power system feasible by 2050?" In: *Applied Energy* 233-234 (2019), pp. 1027–1050. DOI: https://doi.org/10.1016/j.apenergy.2018.08.109.

Appendix A

MATLAB solver

A.1 lsqlin

Multiple solutions As explained in chapter 2, the code makes an extensive use of the *lsqlin* function [21] to solve linear least-squares systems with linear bounds and constraints, the mathematical formulation is recalled here:

$$\min_{x}\left\{\frac{1}{2}\|\boldsymbol{C}\cdot\boldsymbol{x}-\boldsymbol{d}\|_2^2\right\} \quad \text{such that} \begin{cases} \boldsymbol{A}\cdot\boldsymbol{x}\leq\boldsymbol{b} \\ \boldsymbol{A}_{eq}\cdot\boldsymbol{x}=\boldsymbol{b}_{eq} \\ \boldsymbol{l}_b\leq\boldsymbol{x}\leq\boldsymbol{u}_b \end{cases} \tag{A.1.1}$$

This problem is solved by reformulating it in a quadratic programming problem, indeed

$$\frac{1}{2}\|\boldsymbol{C}\boldsymbol{x}-\boldsymbol{d}\|_2^2=\frac{1}{2}(\boldsymbol{C}\boldsymbol{x}-\boldsymbol{d})^T(\boldsymbol{C}\boldsymbol{x}-\boldsymbol{d})=\frac{1}{2}(\boldsymbol{x}^T\boldsymbol{C}^T\boldsymbol{C}\boldsymbol{x}-\boldsymbol{x}^T\boldsymbol{Q}^T\boldsymbol{d}-\boldsymbol{d}^T\boldsymbol{Q}\boldsymbol{x}+\boldsymbol{d}^T\boldsymbol{d})=$$
$$\frac{1}{2}(\boldsymbol{x}^T\boldsymbol{C}^T\boldsymbol{C}\boldsymbol{x}-2\boldsymbol{x}^T\boldsymbol{C}^T\boldsymbol{d}+\boldsymbol{d}^T\boldsymbol{d})$$

since $\boldsymbol{d}^T\boldsymbol{d}$ is a constant term, it is sufficient to solve

$$\min_{x}\left\{F(x)=\frac{1}{2}\boldsymbol{x}^T\boldsymbol{H}\boldsymbol{x}+\boldsymbol{q}^T\boldsymbol{x}\right\} \tag{A.1.2}$$

where $\boldsymbol{H}=\boldsymbol{C}^T\boldsymbol{C}$ and $\boldsymbol{q}=-\boldsymbol{C}^T\boldsymbol{d}$.
$\boldsymbol{H}$ is the Hessian matrix of F and, given the structure of $\boldsymbol{C}$, it can be proven [15] that it is also positive semidefinite, but it is not strictly positive definite. This means that F is convex but not strictly convex, therefore any local minimum of F is also global, but there may be many points of minimum. In particular the following situations can

happen:

- The solution of the system of equations (A.1.1) is unique. In this case the constraints are "strong" in the sense that the solution $\boldsymbol{x}$ lies on some of them and they prevent the residual $\boldsymbol{R} = \boldsymbol{C} - \boldsymbol{d}$ from being null (for instance the demand could not be met, or the residual surplus is greater than zero). Therefore, the technologies of the code section under analysis (generators, storage, transmission lines) are used to minimize the residual in the sense of least squares.
- The residual is zero and there may be several combinations of power flows on the transmission lines and power generated in the various zone that satisfy system (A.1.1). In particular, starting from the same set of inputs, the solver stops always at the same solution within the constraints, but this solution is not predictable (i.e. among all the infinite solution *lsqlin* "chooses" one without a clear logic).

Therefore, the results regarding power flows and generated power in the various zones are in a certain way arbitrary when they do not lie on the constraints. This fact is not a problem when the user is interested only in cumulative quantities such as total energy produced by the various technologies, the LCOTE, etc. But, if the focus is to examine the hourly behaviour of the system, it could be preferable to follow a precise rationale for the choice of $\boldsymbol{x}$ in order to obtain a more significant analysis. Moreover, if line losses are present unmotivated power flows lead to excessive usage of dispatchable energy.

Solver algorithm *lsqlin* provides two iterative algorithms suitable for solving (A.1.1): interior-point and active-set. Interior-point is the default algorithm, and it is actually much faster than active-set for solving COMESE systems of equations. Nevertheless, the latter gives the possibility to specify the starting point ($\boldsymbol{x_0}$) for the iterations and this could lead to a cut in the computational times. Indeed, for every hour of the year, COMESE looks 24 hours in the future to find the optimal dispatchment, therefore it is likely that solution $\boldsymbol{x_{h+1}}$ (which takes into account the hours from $h+1$ to $h+1+25$) is similar to solution $\boldsymbol{x_h}$ (which takes into account the hours from h to $h+25$). Therefore $\boldsymbol{x_h}$ could be a good starting point $\boldsymbol{x_{0,\,h+1}}$. Unfortunately, active-set, to speed up, needs to "know" not only $\boldsymbol{x_0}$, but also other algorithm-specific data from a previous solution, for example which were the active constraints. The MATLAB command *optimwarmstart* [21] carries over this information, but it cannot be used when the set of equality constraints changes, that is our case: going from one hour to the next the $\boldsymbol{A_{eq}}$ matrix changes because, for instance, the equality constraints shift back of one row. In conclusion the interior-point algorithm is the best choice for COMESE.

Solver options This section focuses on the overall behaviour of the code when *lsqlin* options are modified, in particular the *Optimality Tolerance* and *Constraint Tolerance*. The default value of the latter is 10^{-6} and increasing it does not lead to any advantage, on the contrary it can cause convergence problems due to inconsistency of the partial results obtained with the various code sections, and inaccuracy in the final solution. As regards *Optimality Tolerance* several tests were made in order to find a good compromise between computational time and solution accuracy. 10^{-6} turned out to be the best option because choosing smaller values has a strong impact on the computational burden, but the results are practically unaffected. On the other hand, if *Optimality Tolerance* is increased to, for instance, 10^{-4} there is no significant improvement in the running time. Moreover, using even higher values can lead to deceptive results and problems of solver convergence.

Solver flags *lsqlin* provides as one of the outputs a flag which specifies the reason the algorithm stopped: the flags that appear more frequently are summarized in the following table:

flag	message
2	Step size smaller than options, constraints satisfied.
1	optimum found
0	Solver stopped because number of iterations exceeded maximum iterations available.
-2	The problem is infeasible. During presolve, quadprog found the constraints to be inconsistent within the constraint tolerance.
-3	The problem is unbounded. lsqlin appears to have found a feasible direction that causes the objective to decrease without bound.

Table A.1: lsqlin flags

The reasons behind each flag different from 1 have been analysed, in order to find whether is possible to "help" the solver to converge. In general, using dense matrices, although it is less efficient as regards computational time, leads to solving the issue (this feature was already implemented in the code). So are now presented those cases, although rare (a few hours in a year), in which the solver still does not converge. It should be noted that the frequency of appearance of these flags depends on the scenario

under analysis, on the solver options, on how the sections of COMESE are implemented (Power flow, storage), and also on the MATLAB version.

- flag 2. This flag appears when the solver's solution at iteration $n + 1$ is too close, in a relative sense, to the solution at iteration n; so it is more likely to happen if there are some variables in the linear system of order of magnitude very different from the others. In general decreasing the *Step tolerance* option, and relaxing the *Optimally tolerance* parameter, solves this flag.

- flag 0. This flag appears when the solver does not find the optimum within the maximum number of iterations set by the user. As for *flag 2*, usually this is due to the fact that some variables or bounds have an order of magnitude very different from the others. In particular it might happen that certain quantities resulting from a subtraction are very close to zero. So, rounding sufficiently small numbers to zero and decreasing *Optimally tolerance* of one order of magnitude help the solver to converge.

- flag -2. This flag appears when *lsqlin* believes that constraints are inconsistent. This is due to some computational issues because constraints should always be consistent giving the way in which they are defined. It was found that increasing the solver parameter *Constraint tolerance* does not help to solve the problem, instead, if a small quantity is, respectively, subtracted from $\boldsymbol{l_b}$ and added to $\boldsymbol{u_b}$ the solver converges. After some tests, a value of 10^{-5} appears to be sufficient and it does not compromise the accuracy of the solution. On the other hand, when the parameter *Optimality tolerance* is relaxed too much this problem becomes more and more frequent and sometimes insolvable.

- flag -3. Another flag that in principle should never appear because, given the structure of the various code sections, all the variables in A.1.1 are always bounded. Anyway, relaxing the upper and lower bounds as explained in the former point allows to solve this issue the few times it happens.

After each *lsqlin* call, a section was implemented that, based on the flag value obtained, employs one of the actions just explained and attempts to solve the system (A.1.1) again.

Impact of the magnitude of system variables on code speed It was studied how the code responds to an overall change in the size of the system under analysis: this can be helpful to understand whether COMESE is suitable for studying scenarios of different

scales (regional, national, European) and which is the best unit of measurement to use when performing a simulation. Originally the code worked in MW (and MWh) and, for three scenarios under analysis, all the physical quantities were scaled by 100, 10, 1/10, 1/100, 1/1000 (which is equivalent to working in GW). The three test scenarios were created starting from a generic full-renewables Italian scenario already present in the database, let's call it *Scenario-fullresITA*: the first one (*Scenario-Test1*) takes into account only the North and Centre-North zones and the line between them, the second one (*Scenario-Test2*) is exactly *Scenario-fullresITA*, the third one (*Scenario-Test3*) is similar to (*Scenario-Test2*) but with the demand curve scaled by a factor 2, in order to obtain a situation where is very difficult (or impossible) to balance the load. Obviously the computational time depends on the computer used (all the simulations were run on a i7-11th generation 16 GB RAM machine), so it is presented only as a parameter to confront the various alternative. The LCOTE depends on the total energy produced by the various technologies, so it is used to verify that system dimensions do not impact the overall results.

scale factor	time [s]	LCOTE [c€/kWh]
100	700	10,130
10	630	10,130
1	550	10,130
1/10	520	10,130
1/100	500	10,130
1/1000	460	10,130

Table A.2: Scenario-Test1

scale factor	time [s]	LCOTE [c€/kWh]
100	1050	10,233
10	930	10,234
1	760	10,234
1/10	700	10,234
1/100	610	10,234
1/1000	580	10,232

Table A.3: Scenario-Test2

It can be seen that reducing the "size" of the system leads to a decrease in the computational time, and the final results are practically the same: as regards *Scenario-Test2* and

scale factor	time [s]	LCOTE [c€/kWh]
100	1170	11,982
10	990	11,982
1	850	11,982
1/10	940	11,982
1/100	700	11,983
1/1000	660	11,985

Table A.4: Scenario-Test3

Scenario-Test3 the reduction is between 20 and 25 percent when moving from MW to GW, while is a little lower for *Scenario-Test1* (which is the "simplest" scenario). On the other hand increasing the magnitude of the variables has a clear negative impact on the running time. These results were confirmed also when carrying out other tests with other scenarios, so it can be concluded that COMESE is faster when analysing smaller numbers, therefore it was chosen to perform the various simulation using GW as unit of measurement.

A.2 linprog

linprog [21] is the MATLAB function used to solve linear programming problems in the form:

$$\min_{x} \left\{ F(x) = \boldsymbol{f}^T \cdot \boldsymbol{x} \right\} \quad \text{such that} \begin{cases} \boldsymbol{A} \cdot \boldsymbol{x} \leq \boldsymbol{b} \\ \boldsymbol{A_{eq}} \cdot \boldsymbol{x} = \boldsymbol{b_{eq}} \\ \boldsymbol{l_b} \leq \boldsymbol{x} \leq \boldsymbol{u_b} \end{cases} \tag{A.2.1}$$

Since the objective function F is linear and not quadratic as in equation (A.1.2), the computational complexity strongly decreases. Indeed with this formulation (extensively explained in chapter 3.3), the temporal and zonal description of the system is kept only in the constraints, whereas the objective function involves only cumulative quantities, thus reducing the resolution of the model. Anyway, the considerations regarding solver flags and the impact of the magnitude of system variables made above hold also in this case.

Ringraziamenti

Un ringraziamento va al Prof. Zollino, per avermi dato la possibilità di intraprendere questo interessante lavoro di tesi. Inoltre, ringrazio di cuore gli altri membri del gruppo di ricerca, Chiara Bustreo, Marco e Umberto, per avermi guidato in questo percorso ed essere sempre stati disponibili a confrontare nuove idee e a darmi preziosi suggerimenti.
Questi anni a Padova non sarebbero stati gli stessi senza il fantastico gruppo di persone che ho avuto la fortuna di conoscere all'università, e che ringrazio per aver reso questa esperienza unica e indimenticabile.
Ovviamente non posso dimenticare i *Classmeils* di Vittorio, che, nonostante il passare del tempo, continuano ad arricchire le mie giornate e rimangono quel genere di amici su cui sai che puoi e potrai sempre contare. Ad maiora!
Un pensiero particolare va a Borty, comune denominatore tra questi due mondi e che mi ha indissolubilmente accompagnato dalle stelle di San Gregorio alle stalle di . . . beh hai capito ;)
Infine il mio più grande ringraziamento è per i miei genitori e mio fratello, ai quali dedico questa tesi. Mi avete dato e insegnato più di quanto potessi sperare e più di quanto io possa scrivere in queste poche righe.